AVOIDING DISCRETIZATION ISSUES FOR NONLINEAR EIGENVALUE PROBLEMS

MATTHEW J. COLBROOK* AND ALEX TOWNSEND†

Abstract. The first step when solving an infinite-dimensional eigenvalue problem is often to discretize it. We show that one must be extremely careful when discretizing nonlinear eigenvalue problems. Using examples from the NLEVP collection, we demonstrate that discretization can lead to several issues, including: (1) introduction of spurious eigenvalues, (2) omission of spectra, (3) severe ill-conditioning, and (4) emergence of ghost essential spectra. While many eigensolvers are available for solving finite matrix nonlinear eigenvalue problems, we propose InfBeyn, a solver for general holomorphic infinite-dimensional nonlinear eigenvalue problems that circumvents these discretization issues. We prove that InfBeyn is stable and converges. Furthermore, we provide an algorithm that computes the problem's pseudospectra with explicit error control, enabling verification of computed spectra. Both algorithms and numerical examples are publicly available in the `infNEP` software package, which is written in MATLAB.

Key words. Nonlinear eigenproblems, spectral pollution, conditioning, infinite-dimensional linear algebra, pseudospectra

AMS subject classifications. 35P30, 65N25, 65N30, 47A10

1. Introduction. Many nonlinear eigenvalue problems (NEPs) arise from discretizing an infinite-dimensional problem. In fact, 25 out of the 52 NEPs from the NLEVP collection are derived by discretizing a continuous problem such as a differential eigenvalue problem [4]. The analysis typically centers on how to solve the resulting finite-dimensional NEP after discretization. However, as we show in this paper, discretizing an infinite-dimensional NEP can introduce serious problems. It can modify, destabilize, or destroy the desired eigenvalues, leading to the computed eigenvalues misrepresenting those of the underlying continuous problem - Table 1.1 presents a list of issues that we demonstrate in section 4 for six examples.

Given a domain (a non-empty, open, and connected subset) $\Omega \subset \mathbb{C}$ and a matrix-valued function $F : \Omega \to \mathbb{C}^{n\times n}$, the matrix NEP consists of finding eigenvalues $\lambda \in \Omega$ and nonzero eigenvectors $v \in \mathbb{C}^n$ so that $F(\lambda)v = 0$. There are many applications of NEPs in mechanical vibrations [65], fluid-solid interactions [96], photonic crystals [80], time-delay systems [55], resonances [9], and numerous other areas [64,69,85]. Many of these matrix NEPs are derived from discretizing differential operators, where nonlinearities arise from eigenvalue-dependent boundary conditions [12], material parameters [37]; particular basis functions [5], or truncating an infinite domain with transparent boundary conditions [66].

In this paper, we propose a solver for infinite-dimensional NEPs, which is a variant of the contour-based algorithm called Beyn's method [6]. Rather than first discretizing the NEP, our algorithm delays discretization until the last possible moment. By delaying discretization, we avoid modifying, destabilizing, and destroying eigenvalues and provably compute them accurately.

1.1. NEPs on Hilbert spaces. We consider two separable Hilbert spaces $\mathcal{H}_1$ and $\mathcal{H}_2$ with inner products $\langle\cdot,\cdot\rangle_{\mathcal{H}_j}$ and norms $\|\cdot\|_{\mathcal{H}_j}$, and a scalar-dependent operator

$$T(\lambda) : \mathcal{D}(T) \supseteq \mathcal{H}_1 \to \mathcal{H}_2.$$

*DAMTP, University of Cambridge, Cambridge, CB3 0WA. (m.colbrook@damtp.cam.ac.uk)
†Department of Mathematics, Cornell University, Ithaca, NY 14853. (townsend@cornell.edu)

TABLE 1.1
Discretization issues encountered in our six examples from the NLEVP collection. Our proposed InfBeyn algorithm avoids these issues using an infinite-dimensional approach (see subsection 2.2).

Example	Observed discretization woes
`acoustic_wave_1d`	spurious eigenvalues slow convergence
`acoustic_wave_2d`	spurious eigenvalues wrong multiplicity
`butterfly`	spectral pollution missed spectra wrong pseudospectra
`damped_beam`	slow convergence resolved eigenfunctions with inaccurate eigenvalues
`loaded_string`	ill-conditioning from discretization
`planar_waveguide`	collapse onto ghost essential spectrum failure for accumulating eigenvalues spectral pollution

For each fixed λ, $T(\lambda)$ is a closed and densely-defined linear operator acting on the Hilbert space $\mathcal{H}_1$. However, we allow nonlinear dependence on the parameter λ. We assume that $T(\lambda)$ has a fixed densely-defined domain $\mathcal{D}(T) \subset \mathcal{H}_1$. For a domain $\Omega \subset \mathbb{C}$, we assume that the map $\Omega \ni \lambda \mapsto T(\lambda)u \in \mathcal{H}_2$ is holomorphic for each fixed $u \in \mathcal{D}(T)$ [59, p. 375].[1] We focus on NEPs that involve finding eigenvalues $\lambda \in \mathbb{C}$ and nonzero eigenfunctions $u \in \mathcal{D}(T)$ such that

$$T(\lambda)u = 0. \tag{1.1}$$

We call u an "eigenfunction" to distinguish it from the finite-dimensional case, even though $\mathcal{H}_1$ may not be a function space. These assumptions extend the usual assumptions for matrix NEPs [47] and allow us to develop a contour-based eigensolver for (1.1). Many families of NEPs satisfy these assumptions, such as boundary NEPs for partial differential equations, where the variable coefficients and boundary conditions depend holomorphically on the eigenvalue parameter λ [73, 84].

The *spectrum* of T, denoted by $\Lambda(T)$, is the set of points $\lambda \in \Omega$ such that $T(\lambda) : \mathcal{D}(T) \to \mathcal{H}_2$ is not boundedly invertible. The *resolvent set* $\rho(T) = \Omega \setminus \Lambda(T)$ is relatively open in Ω and $T(z)^{-1}$ is bounded holomorphic for $z \in \rho(T)$. For any $z \in \rho(T)$, the resolvent operator is $T(z)^{-1} : \mathcal{H}_2 \to \mathcal{D}(T) \subset \mathcal{H}_1$. Because we deal with operators acting on infinite-dimensional spaces, $\Lambda(T)$ may contain points that are not eigenvalues. Namely, in general,

$$\left\{\lambda \in \Omega \,\middle|\, \ker(T(\lambda)) \neq \{0\}\right\} \subsetneq \Lambda(T).$$

This situation can be avoided under the assumption of Fredholmness. A closed linear operator $S : \mathcal{D}(S) \supset \mathcal{H}_1 \to \mathcal{H}_2$ is Fredholm if its range is closed and its kernel and cokernel have finite dimension. Its Fredholm index is $\dim(\ker(S)) - \dim(\operatorname{coker}(S))$ [39,

[1] While the assumption that $\lambda \mapsto T(\lambda)u$ is holomorphic for each λ uses a fixed domain $\mathcal{D}(T)$, it captures eigenvalue-dependent boundary conditions by combining the differential operator and the boundary operator to a two-component operator defined on a fixed space [81].

p. 372]. If $T(\lambda)$ is a (possibly unbounded) *Fredholm operator* for each $\lambda \in \Omega$ and $\Lambda(T) \neq \Omega$, then $\Lambda(T)$ consists of isolated points that are eigenvalues with finite algebraic and geometric multiplicities, and $T(\lambda)$ has Fredholm index zero for all $\lambda \in \Omega$ [44]. Under these assumptions, many finite-dimensional NEP theorems have an infinite-dimensional analogue [57]. For example, a version of Keldysh's theorem for infinite-dimensional NEPs (see Theorem 2.1) underpins our contour-based NEP solver. Since Fredholm operators remain Fredholm after small perturbations [58, Thm. 1], our assumptions are not brittle and allow for the design of numerical methods. The set of points $\lambda \in \Omega$ that are non-isolated points of $\Lambda(T)$ or for which $T(\lambda)$ is not Fredholm is known as the *essential spectrum*.

1.2. Woes of discretization. While problems caused by discretization appear to be common folklore, there is no systematic study of their effects on NEPs. We look at several examples for a lucid illustration (see section 4). There are several troubling problems caused by the discretization of NEPs that deserve careful attention:

- **Spurious eigenvalues.** Spurious eigenvalues unrelated to the infinite-dimensional problem may arise due to discretization. These spurious eigenvalues can remain even as the discretization size increases to infinity, a phenomenon known as *spectral pollution*. This can occur even when the spectrum is purely discrete.
- **Spectral invisibility.** *Spectral invisibility* refers to some (or all) of the eigenvalues of the NEP being missed by the discretization, even as the discretization size increases to infinity. Regions of spectra can be "invisible" to discretizations.
- **Ill-conditioning.** The infinite-dimensional NEP may have well-conditioned eigenvalues, while the discretized problem has ill-conditioned eigenvalues. Hence, no, even stable, finite-dimensional solver can overcome this issue post-discretization.
- **Exceedingly slow convergence.** In practice, we desire that the eigenvalues of the discretization rapidly converge to those of the infinite-dimensional problem. If one has slow convergence, it can be computationally prohibitive to compute eigenvalues representing the infinite-dimensional ones. Even if eigenfunctions are resolved accurately, the corresponding eigenvalues may be inaccurate.
- **Wrong multiplicity.** Eigenvalues of the infinite-dimensional problem may be well-approximated using discretizations but with the wrong multiplicity.
- **Accumulating eigenvalues.** The discrete spectrum can accumulate at the essential spectrum. This can be challenging for discretizations to resolve accurately.
- **Ghost essential spectra.** Many infinite-dimensional NEPs with discrete spectra arise from an underlying spectral problem that has essential spectra. For example, this is common in domain truncation for resonance computations. The eigenvalues of the discretized NEP may collapse onto the *ghost essential spectrum* of the underlying problem.

We note that while many of these issues also appear in linear spectral problems, nonlinearity in the spectral parameter can make these challenges more pronounced.

1.3. Contributions. To overcome these discretization issues, we introduce an infinite-dimensional analog of Beyn's method [6, 7] (see subsection 2.2). We call our algorithm InfBeyn (see subsection 2.2), which is based on contour integration and adaptively discretizes only linear equations.[2] It computes eigenvalues inside a region in the complex plane by integrating along the region's boundary. It forms a

[2]The ease of using adaptive discretizations as part of a contour method depends on the setup. For example, with spectral methods, it is straightforward. For more complicated discretizations, such as adaptive finite elements, one would need to carry out transformations between meshes.

small generalized matrix eigenvalue problem whose eigenvalues match those of the infinite-dimensional NEP inside the contour. While previous approaches to infinite-dimensional NEPs are predominantly problem-specific, InfBeyn provides a general method that converges for any holomorphic NEP in regions where the spectrum is discrete. Moreover, we use techniques from infinite-dimensional randomized numerical linear algebra to prove that the method converges and is stable. Proving convergence and stability is a well-known problem for contour-based methods for finite-dimensional problems, but it is manageable in infinite dimensions.

The term *spectral exactness* is commonly used to mean approximation without spectral pollution or invisibility [1]. A version of Beyn's method has been developed for bounded Fredholm pencils in [7]. The setup of [7] uses the discrete convergence theory of [93] applied to domain truncation of differential operators on $L^2(\mathbb{R})$. The assumptions needed are strong and already imply spectral exactness [94]. In contrast, our solve-then-discretize[3] approach only requires convergence of solutions of linear systems corresponding to the resolvent, which is a much weaker assumption. When studying spectral exactness, it is common to study the convergence of the resolvents of operators [59, Sections IV.2, VIII.1], [79, Theorems VIII.23–25], [100, Section 9.3]. One may vary the spaces in which the operators are defined by embedding all spaces in a larger one and considering the "generalized" convergence of the lifted resolvents. Typically, it is much easier for a discretization method to converge when solving linear systems than to have spectral exactness. Generalized strong resolvent convergence does not imply the absence of spectral pollution, even if all the operators are self-adjoint with compact resolvent [15, Example 5]. In the self-adjoint case, generalized strong resolvent convergence implies the absence of spectral invisibility [10, Theorem 2.4]. However, in the non-self-adjoint case, not even norm resolvent convergence implies the absence of spectral invisibility [59, Example IV.3.8]. We can obtain convergence to the spectrum for contour methods by allowing the discretization sizes used at quadrature points to be adaptive. In other words, we convert convergence of the resolvent to convergence of the spectrum.

In addition to computing eigenvalues of infinite-dimensional NEPs, we also compute pseudospectral sets to give us a more comprehensive understanding of the stability of a system's spectrum (see subsection 2.3). Discretizing NEPs can also cause issues here (see subsection 4.3), and the pseudospectral sets for a discretization may be misleading, even when spectral pollution and invisibility do not occur (see subsection 2.3.1). We provide the first general algorithm that converges to the pseudospectra of NEPs, even when the spectrum is not discrete. Moreover, the algorithm's output is guaranteed to be inside the true pseudospectral sets, thus directly verifying the computation and allowing aposterior verification of the eigenvalues computed by InfBeyn.

1.4. Outline of paper. The paper is structured as follows: In section 2, we detail infinite-dimensional tools for NEPs, including Keldysh's theorem, our InfBeyn algorithm, and how to compute pseudospectra. In section 3, we analyze the stability of InfBeyn by deriving pseudospectral set inclusions. In section 4, we cover six examples from the NLEVP collection derived from infinite-dimensional NEPs and illustrate discretization woes. We conclude and point to future developments in section 5. To accompany this paper, we have developed a publicly available MATLAB package, `infNEP`, available at [24], which includes all of the examples and figures of this paper.

[3] The "solve-then-discretize" paradigm has recently been applied to spectral computations [23,27, 30,54], extensions of classical methods such as the QL and QR algorithms [26,98], Krylov methods [38,75,95], semigroups [22], and spectral measures [21,29,99].

2. Computational tools for infinite-dimensional NEPs. We first state Keldysh's Theorem (see Theorem 2.1) before describing our infinite-dimensional analog for Beyn's method (see subsection 2.2) and procedure for computing pseudospectra (see subsection 2.3). Rather than directly discretizing the NEP, we delay discretization until the last possible moment and only discretize linear equations.

2.1. Keldysh's theorem. For contour-based methods for NEPs, Keldysh's theorem is an important expansion used to reduce the NEP to a linear generalized matrix eigenvalue problem. Its original form goes back to Keldysh [60, 61], with numerous generalizations [40, 68, 72, 92]. For a comprehensive discussion and proof of Keldysh's theorem on Banach spaces, see [63, Appendix A]. We state the theorem for the general case of unbounded operators and provide a proof for completeness.

THEOREM 2.1. *Let $\Omega \subset \mathbb{C}$ be a domain and T in (1.1) be such that $\Omega \ni \lambda \mapsto T(\lambda)u$ is holomorphic for each $u \in \mathcal{D}(T)$, $T(\lambda)$ is Fredholm for all $\lambda \in \Omega$, and $\Lambda(T) \neq \Omega$. Suppose the set of eigenvalues $\Lambda(T) = \{\lambda_1, \dots, \lambda_s\}$ is finite and m is the sum of their algebraic multiplicities. Then, for each λ_i, there exists*

$$\{v_k^{ij} \,|\, 0 \le k \le m_{ij}-1, 1 \le j \le d_i\} \subset \mathcal{H}_1, \quad \{w_k^{ij} \,|\, 0 \le k \le m_{ij}-1, 1 \le j \le d_i\} \subset \mathcal{H}_2$$

that are canonical Jordan chains for T and T^* at λ, respectively, with normalization

$$\sum_{\alpha=0}^{k} \sum_{\beta=1}^{m_{ip}} \frac{\left\langle \frac{\mathrm{d}^{(\alpha+\beta)}T}{\mathrm{d}\lambda^{(\alpha+\beta)}}(\lambda) v_{m_{ip}-\beta}^{ip}, w_{k-\alpha}^{iq} \right\rangle_{H_2}}{(\alpha+\beta)!} = \delta_{pq}\delta_{0k}, \quad 0 \le k \le m_{iq}-1, \quad 1 \le p,q \le d_i,$$

such that the resolvent of T can be decomposed as

$$T(z)^{-1} = V(zI-J)^{-1}W^* + R(z) \quad \forall z \in \rho(T). \tag{2.1}$$

Here,

$$V_{ij} = \left[v_0^{ij}, v_1^{ij}, \dots, v_{m_{ij}-1}^{ij}\right], \quad W_{ij} = \left[w_{m_{ij}-1}^{ij}, w_{m_{ij}-2}^{ij}, \dots, w_0^{ij}\right],$$

J_{ij} is a $m_{ij} \times m_{ij}$ Jordan block with eigenvalues λ_i,

$$V_{\lambda_i} = [V_{i1}, \dots, V_{id_i}], \quad W_{\lambda_i} = [W_{i1}, \dots, W_{id_i}], \quad J_{\lambda_i} = \operatorname{diag}(J_{i1}, \dots, J_{id_i}),$$
$$V = [V_{\lambda_1}, \dots, V_{\lambda_s}], \quad W = [W_{\lambda_1}, \dots, W_{\lambda_s}], \quad J = \operatorname{diag}(J_{\lambda_1}, \dots, J_{\lambda_s}) \in \mathbb{C}^{m \times m},$$

and $R(z) : \mathcal{H}_2 \to \mathcal{H}_1$ is a holomorphic remainder.

Proof. Fix any point $\lambda_0 \in \Omega$ and consider $\mathcal{H}_1' = \mathcal{D}(T)$ with inner product $\langle x, y\rangle_{\mathcal{H}_1} + \langle T(\lambda_0)x, T(\lambda_0)y\rangle_{\mathcal{H}_2}$, which induces the graph norm. The space $\mathcal{H}_1'$ is a Hilbert space since $T(\lambda_0)$ is a closed operator. We regard each $T(\lambda)$ as an operator from $\mathcal{H}_1'$ to $\mathcal{H}_2$. Since $T(\lambda)$ is defined on the whole of $\mathcal{H}_1'$, it is bounded for any $\lambda \in \Omega$. The spectrum of T is unchanged when considering $\mathcal{H}_1'$, $T(\lambda)$ is still Fredholm and $\Omega \ni \lambda \mapsto T(\lambda)u$ is holomorphic for each fixed $u \in \mathcal{D}(T) = \mathcal{H}_1'$.

We apply [73, Thm. 1.6.5] to the bounded family $T(\lambda) : \mathcal{H}_1' \to \mathcal{H}_2$ to find that

$$T(z)^{-1} = V_{\lambda_i}(zI - J_{\lambda_i})^{-1}W_{\lambda_i}^* + R_{\lambda_i}(z) \quad \forall z \in \rho(T), \quad i = 1, \dots, s,$$

where the remainder $R_{\lambda_i} : \mathcal{H}_2 \to \mathcal{H}_1'$ is holomorphic on $(\Omega \backslash \Lambda(T)) \cup \{\lambda_i\}$. Since the norm of $\mathcal{H}_1'$ dominates that of $\mathcal{H}_1$, R_{λ_i} is holomorphic as a map into $\mathcal{H}_1$. Note that

$$R(z) := T(z)^{-1} - \sum_{i=1}^{s} V_{\lambda_i}(zI - J_{\lambda_i})^{-1}W_{\lambda_i}^* = T(z)^{-1} - V(zI-J)^{-1}W^*$$

is holomorphic on $\Omega\backslash\Lambda(T)$. Moreover, for any i, $R(z) = R_{\lambda_i}(z) - \sum_{j\neq i}^{s} V_{\lambda_j}(zI - J_{\lambda_j})^{-1}W_{\lambda_j}^*$ is holomorphic in a neighborhood of λ_i. The statement of the theorem follows. ∎

The forms of V, W, and J (along with the definition of canonical Jordan chains) directly generalize the matrix case [47, Sec. 2.4]. The assumption of finitely many eigenvalues can always be met by restricting Ω to a smaller domain of interest, if necessary. The expansion in (2.1) shows that $T(z)^{-1}$ can be expressed in terms of $(zI - J)^{-1}$ up to a holomorphic remainder. This decomposition allows for the use of contour integration involving $T(z)^{-1}$ to formulate an $m \times m$ generalized eigenvalue problem that shares the same eigenvalues as (1.1) within Ω.

2.2. An infinite-dimensional analogue of Beyn's method. Beyn's method is efficient for solving matrix NEPs and is particularly useful when one wants to compute eigenvalues inside a known region [6]. This contour-based method uses Keldysh's expansion in (2.1) to compute a smaller linear pencil whose spectral properties match those of the original problem inside the region enclosed by the contour. If $F(z) \in \mathbb{C}^{n\times n}$ is a matrix NEP, then it first computes the following two matrices:

$$A_0 = \frac{1}{2\pi i}\int_\Gamma F(z)^{-1}G\,\mathrm{d}z, \qquad A_1 = \frac{1}{2\pi i}\int_\Gamma zF(z)^{-1}G\,\mathrm{d}z, \tag{2.2}$$

where Γ is a closed rectifiable Jordan curve inside Ω enclosing m eigenvalues of $F(z)$ (counted via algebraic multiplicity). Here, $G \in \mathbb{C}^{n\times(m+p)}$ is a matrix with $m \ll n$ that is often selected at random with independent standard Gaussian entries, and p is a small oversampling factor (e.g., $p = 5$) that we recommend for the robustness of the method. After computing A_0 and A_1, Beyn's method solves an $m \times m$ generalized matrix eigenvalue problem related to A_0 and A_1.

The usual way to apply Beyn's method is to discretize the NEP and then use Beyn's method. The dominating computational cost of Beyn's method is solving linear systems. However, we prefer an infinite-dimensional analog of Beyn's method, which we now describe, to overcome discretization concerns. There are three essential ingredients to Beyn's method, which we generalize in turn:

(i) **Randomly generated test functions.** Beyn's method uses a random matrix $G \in \mathbb{C}^{n\times(m+p)}$ whose columns are standard Gaussian test vectors. A function, g, drawn from a Gaussian process (GP) is an infinite-dimensional analog of a vector drawn from a multivariate Gaussian distribution in the sense that samples from g follow a multivariate Gaussian distribution [13].[4] We describe the process for $\mathcal{H}_2 = L^2(\mathcal{X})$ on a domain $\mathcal{X} \subseteq \mathbb{R}^d$ and the process is analogous for other Hilbert spaces. We write $g \sim \mathcal{GP}(0, K)$ for some continuous positive definite kernel $K : \mathcal{X}\times\mathcal{X} \to \mathbb{R}$ if for any $x_1, \ldots, x_k \in \mathcal{X}$, $(g(x_1), \ldots, g(x_k))$ follows a multivariate Gaussian distribution with mean $(0, \ldots, 0)$ and covariance $K_{ij} = K(x_i, x_j)$ for $1 \le i, j \le k$. We typically use the squared exponential covariance kernel given by

$$K_{\mathrm{SE}}(x, y) = \frac{1}{\mu\sqrt{2\pi}}\exp\left(-(x-y)^2/(2\mu^2)\right), \qquad \mu > 0, \tag{2.3}$$

where $s_\mu = \mu\sqrt{2\pi}$ is a scaling factor. The length scale parameter μ determines the correlation between samples of g. If μ is large, the samples $g(x_1), \ldots, g(x_k)$ are

[4] Using functions drawn from a Gaussian process here is certainly not the only way to go. However, this distribution of functions has become popular because of the underlying explicit probability estimates that can be derived from the randomized SVD theory [13, 49].

Algorithm 2.1 InfBeyn: Our infinite-dimensional Beyn's method for NEPs.

Input: Nonlinear eigenvalue problem $T(z)u = 0$, contour Γ enclosing m eigenvalues.

1: Draw a $\mathcal{X} \times (m+p)$ quasimatrix whose columns are independently drawn from the Gaussian process $\mathcal{GP}(0, K_{\mathrm{SE}})$.
2: Compute quasimatrices A_0 and A_1 in (2.4) with a quadrature rule (2.7).
3: Compute the m-truncated SVD of A_0 in (2.5).
4: Form and solve the $m \times m$ generalized eigenvalue problem in (2.6) for eigenvalues λ_j and eigenvectors $x_j \in \mathbb{C}^m$.

Output: Eigenvalues $\lambda_1, \ldots, \lambda_m$ in Ω and eigenfunctions $u_j = \mathcal{U}\Sigma_0 x_j$.

highly correlated, and g is close to a constant function. If μ is small, then samples of g are only weakly correlated, and g is usually a highly oscillatory function. We use $\mathcal{GP}(0, K_{\mathrm{SE}})$ to generate random functions in InfBeyn.

(ii) **Contour integration.** InfBeyn computes the following two quasimatrices:[5]

$$A_0 = \frac{1}{2\pi i}\int_\Gamma T(z)^{-1}\mathcal{G}\,\mathrm{d}z, \qquad A_1 = \frac{1}{2\pi i}\int_\Gamma zT(z)^{-1}\mathcal{G}\,\mathrm{d}z, \tag{2.4}$$

where $\mathcal{G}$ is a $\mathcal{X} \times (m+p)$ quasimatrix with each column a function independently drawn from $\mathcal{GP}(0, K_{\mathrm{SE}})$.

(iii) **Solving a generalized matrix eigenvalue problems.** In InfBeyn, A_0 and A_1 are quasimatrices with $m+p$ columns. The related $m \times m$ linear pencil is constructed using the economized singular value decomposition (SVD) of A_0 [89, Sec. 4], i.e.,

$$A_0 = \mathcal{U}\Sigma_0 V_0^*, \tag{2.5}$$

where $\mathcal{U}$ is a quasimatrix with m orthonormal columns in $L^2(\mathcal{X})$ and $V_0 \in \mathbb{C}^{(m+p)\times m}$ is a matrix with orthonormal columns. We then solve the following $m \times m$ generalized eigenvalue problem:

$$\mathcal{U}^* A_1 V_0 x = \lambda \Sigma_0 x, \qquad x \neq 0. \tag{2.6}$$

For practical computation, InfBeyn approximates the contour integral in (2.4) with a quadrature rule such as a mapped trapezoidal rule. Given a quadrature rule with nodes $z_1, \ldots, z_\ell$ and weights $w_1, \ldots, w_\ell$, we use the approximations

$$\tilde{A}_0 = \frac{1}{2\pi i}\sum_{k=1}^{\ell} w_k T(z_k)^{-1}\mathcal{G} \approx A_0, \qquad \tilde{A}_1 = \frac{1}{2\pi i}\sum_{k=1}^{\ell} w_k z_k T(z_k)^{-1}\mathcal{G} \approx A_1. \tag{2.7}$$

Since $\operatorname{rank}(A_j) = m$, $\sigma_{m+1}(\tilde{A}_j) \approx 0$ for $j = 0, 1$. By performing an m-truncated SVD, we ensure that $\tilde{A}_j$ is of rank m for $j = 0, 1$. The approach is summarized Algorithm 2.1 for the case of simple eigenvalues. In the general case, InfBeyn recovers an $m \times m$ linear pencil (2.6) with the same spectral properties as T inside Γ.

For most of the examples in this paper, computing $T(z)^{-1}\mathcal{G}$ involves solving a linear differential equation with $m+p$ right-hand sides. We do this by adaptively discretizing the differential equations and solving a linear system [76]. For an alternative way to perform the verification step based on computing norms in Chebfun, see [46]. To refine the accuracy of the final computed eigenvalues while keeping computational

[5] A quasimatrix is a matrix whose columns are functions instead of vectors. A $\mathcal{X} \times m$ quasimatrix has m columns, and each column is a function defined on $\mathcal{X}$.

costs low, we first compute a rough estimate of the eigenvalues to isolate them inside a small circular contour. Then, we repeat InfBeyn on each eigenvalue or a small cluster of eigenvalues. There are two reasons for this approach. First, we found this approach more computationally efficient than increasing the oversampling parameter p or the number of quadrature nodes ℓ. Second, the analysis in section 3 reveals that this is an important strategy for NEPs since the matrix VW^* from (2.1) may become ill-conditioned or rank degenerate if the contour is too large.

Several techniques exist for estimating the number of eigenvalues m [33,62]. Consequently, we assume that m is known throughout the paper and focus on the algorithmic and theoretical aspects of our infinite-dimensional analog of Beyn's method.

2.3. Pseudospectra for nonlinear eigenvalue problems. Pseudospectral sets are a mathematical quantity that provides insight into the stability of linear and nonlinear systems, including eigenvalue problems [91]. Consider the set of bounded holomorphic perturbations of T of norm at most $\epsilon > 0$, i.e.,

$$\mathcal{A}(\epsilon) = \left\{ E : \Omega \to \mathcal{B}(\mathcal{H}_1, \mathcal{H}_2) \text{ holomorphic} \,\middle|\, \sup_{z\in\Omega} \|E(z)\| < \epsilon \right\}, \tag{2.8}$$

where $\mathcal{B}(\mathcal{H}_1, \mathcal{H}_2)$ denotes the space of bounded linear maps from $\mathcal{H}_1$ to $\mathcal{H}_2$. The ϵ-pseudospectrum of T is the following union of spectra of perturbed operators:

$$\Lambda_\epsilon(T) := \bigcup_{E\in\mathcal{A}(\epsilon)} \Lambda(T+E).$$

One can show that the set $\Lambda_\epsilon(T)$ remains unchanged if we drop the condition that perturbations are holomorphic. It is also common to consider structured perturbations [43, 53, 74, 88, 97], which can additionally be dealt with using the infinite-dimensional techniques we describe in this section.

For linear matrix eigenvalue problems, if the pseudospectra are small around an eigenvalue, small perturbations do not perturb that eigenvalue very far. However, if the pseudospectra are large around an eigenvalue, then a small perturbation can cause that eigenvalue to move far away from its original position. A similar interpretation exists for NEPs in regions where $\Lambda(T)$ is discrete. That is, for sufficiently small ϵ (so that the spectrum remains discrete under perturbations), $\Lambda_\epsilon(T)$ can be equivalently defined via a backward error, i.e.,

$$\Lambda_\epsilon(T) = \inf\left\{ z \in \Omega \,\middle|\, \eta_T(z) < \epsilon \right\},$$

where $\eta_T(z)$ is a backward error defined in [51,87]:

$$\eta_T(z) = \inf\left\{ \epsilon \,\middle|\, \ker(T(z) + E(z)) \neq \{0\}, \|E\| \leq \epsilon \right\}.$$

An alternative characterization of $\Lambda_\epsilon(T)$ also holds when the spectrum is not discrete. The following is a straightforward generalization of [8, Prop. 4.1] and [74, Thm. 1] to infinite dimensions:

THEOREM 2.2. *Let $\epsilon > 0$. With perturbations measured as in (2.8), we have*

$$\Lambda_\epsilon(T) = \left\{ z \in \Omega \,\middle|\, \|T(z)^{-1}\|^{-1} < \epsilon \right\},$$

where we define $\|T(z)^{-1}\|^{-1} = 0$ if $z \in \Lambda(T)$.

Proof. Suppose that $z \notin \Lambda(T)$ and $\|T(z)^{-1}\|^{-1} < \epsilon$. Then, there exists a vector $v \in \mathcal{H}_2$ of unit norm with $\|T(z)^{-1}v\|_{\mathcal{H}_1} > \epsilon^{-1}$. Let $u = T(z)^{-1}v \in \mathcal{H}_1$ and define the operator $E : \mathcal{H}_1 \to \mathcal{H}_2$ by $E = -vu^*/\|u\|^2_{\mathcal{H}_1}$. Then, $\|E\| = 1/\|u\|_{\mathcal{H}_1} < \epsilon$ and

$[T(z)+E]u=0$ so $z\in\Lambda_\epsilon(T)$. Hence, we find that

$$\left\{z\in\Omega\,\middle|\,\|T(z)^{-1}\|^{-1}<\epsilon\right\}\subset\Lambda_\epsilon(T).$$

For the reverse set inclusion, suppose for a contradiction that $z\in\Lambda_\epsilon(T)$ but that $\|T(z)^{-1}\|^{-1}\geq\epsilon$. Then $z\in\Lambda(T+E)$, for some $E\in\mathcal{A}(\epsilon)$ and hence

$$\|T(z)^{-1}E(z)\|\leq\|T(z)^{-1}\|\|E(z)\|\leq\|E(z)\|/\epsilon<1.$$

Note that $T(z)+E(z)=T(z)(I+T(z)^{-1}E(z))$. Using a Neumann series, we have

$$(I+T(z)^{-1}E(z))^{-1}=\sum_{j=0}^{\infty}(-1)^j[T(z)^{-1}E(z)]^j,$$

which converges because $\|T(z)^{-1}E(z)\|<1$. Hence, since $T(z)$ is invertible, so too is the product $T(z)(I+T(z)^{-1}E(z))$. It follows that $z\notin\Lambda(T+E)$, which is a contradiction. ∎

Theorem 2.2 leads to a method for computing $\Lambda_\epsilon(T)$ that avoids discretization issues. Let $\{\mathcal{P}_n\}$ and $\{\mathcal{Q}_n\}$ be sequences of increasing finite-rank orthogonal projections on $\mathcal{H}_1$ and $\mathcal{H}_2$, respectively, such that $\lim_{n\to\infty}\mathcal{P}_n^*\mathcal{P}_nu=u$ for any $u\in\mathcal{H}_1$ and $\lim_{n\to\infty}\mathcal{Q}_n^*\mathcal{Q}_nv=v$ for any $v\in\mathcal{H}_2$. Letting $\mathcal{R}$ denote the range of an operator, we assume that $\cup_{n\in\mathbb{N}}\mathcal{R}(\mathcal{P}_n)$ and $\cup_{n\in\mathbb{N}}\mathcal{Q}(\mathcal{P}_n)$ form a core of $T(z)$ and $T(z)^*$, respectively, for any $z\in\Omega$. Then, we consider the function

$$\gamma_n(z,T):=\min\left\{\sigma_{\inf}(T(z)\mathcal{P}_n^*),\sigma_{\inf}(T(z)^*\mathcal{Q}_n^*)\right\},\tag{2.9}$$

where $\sigma_{\inf}$ denotes the smallest singular value. The following theorem shows how these functions approximate $\|T(z)^{-1}\|^{-1}$ and hence can be used to compute pseudospectra. The final statement is significant because it shows that in regions of discrete spectra, we only need to consider the functions $\sigma_{\inf}(T(z)\mathcal{P}_n^*)$.

THEOREM 2.3. *The functions γ_n satisfy*

$$\gamma_n(z,T)\geq\|T(z)^{-1}\|^{-1}\quad\textit{and}\quad\lim_{n\to\infty}\gamma_n(z,T)=\|T(z)^{-1}\|^{-1},$$

where the convergence is monotonic from above and uniform on compact subsets of Ω. Moreover, if $z\in\rho(T)\cup\partial\Lambda(T)$, then the same conclusion holds with $\gamma_n(z,T)$ replaced by $\sigma_{\inf}(T(z)\mathcal{P}_n^*)$.

Proof. We first claim that

$$\|T(z)^{-1}\|^{-1}=\min\left\{\sigma_{\inf}(T(z)),\sigma_{\inf}(T(z)^*)\right\},\tag{2.10}$$

where for an unbounded operator $S:\mathcal{D}(S)\supseteq\mathcal{H}_1\to\mathcal{H}_2$,

$$\sigma_{\inf}(S)=\inf\{\|Su\|_{\mathcal{H}_2}\,|\,u\in\mathcal{D}(S),\|u\|_{\mathcal{H}_1}=1\}.$$

To see this, suppose first that $z\notin\Lambda(T)$. Let $u\in\mathcal{D}(T)$ with $\|u\|_{\mathcal{H}_1}=1$, then

$$1=\|u\|_{\mathcal{H}_1}=\|T(z)^{-1}T(z)u\|_{\mathcal{H}_1}\leq\|T(z)^{-1}\|\|T(z)u\|_{\mathcal{H}_2}.$$

Taking the infinum over u yields $\sigma_{\inf}(T(z))\geq\|T(z)^{-1}\|^{-1}$. Conversely, for any $v\in\mathcal{H}_2$ with $\|v\|_{\mathcal{H}_2}=1$, we have

$$1=\|v\|_{\mathcal{H}_2}=\|T(z)T(z)^{-1}v\|_{\mathcal{H}_2}\geq\sigma_{\inf}(T(z))\|T(z)^{-1}v\|_{\mathcal{H}_2}.$$

We now choose a sequence v_n with $\|T(z)^{-1}v_n\|_{\mathcal{H}_2}\to\|T(z)^{-1}\|$ to see that $\sigma_{\inf}(T(z))\leq\|T(z)^{-1}\|^{-1}$. Applying this result to the adjoint yields $\sigma_{\inf}(T(z)^*)=\|T(z)^{*^{-1}}\|^{-1}$.

However, we have $T(z)^{*-1} = (T(z)^{-1})^*$ and hence $\|T(z)^{*-1}\|^{-1} = \|T(z)^{-1}\|^{-1}$. Now suppose that $z \in \Lambda(T)$ and that, for a contradiction, both of $\sigma_{\inf}(T(z))$ and $\sigma_{\inf}(T(z)^*)$ are non-zero. Let $v \in \mathcal{R}(T(z))$ with $\|v\|_{\mathcal{H}_2} = 1$, then the above computation shows that $1 \geq \sigma_{\inf}(T(z))\|T(z)^{-1}v\|_{\mathcal{H}_2}$. It follows that $T(z)^{-1} : \mathcal{R}(T(z)) \to \mathcal{D}(T)$ is bounded. Since $\mathcal{R}(T(z))^\perp = \ker(T(z)^*) = \{0\}$, the range of $T(z)$ is dense in $\mathcal{H}_2$ and hence $T(z)^{-1}$ extends to a bounded operator on $\mathcal{H}_2$. Clearly, $T(z)T(z)^{-1}$ is the identity on $\mathcal{H}_2$. Closedness of $T(z)$ shows that $T(z)^{-1}T(z)$ on $\mathcal{D}(T)$ and hence $z \notin \Lambda(T)$, the required contradiction. The characterization in (2.10) now follows.

Since $T(z)^{-1}$ is bounded holomorphic on $\rho(T)$, $\|T(z)^{-1}\|^{-1}$ is continuous on $\rho(T)$. We show that $\|T(z)^{-1}\|^{-1}$ is continuous on the whole of Ω. Let $z_n \in \rho(T)$ with $z_n \to z \in \Lambda(T)$. If $\sigma_{\inf}(T(z)) = 0$, then for any $\epsilon > 0$, there exists $u_\epsilon \in \mathcal{D}(T)$ of unit norm such that $\|T(z)u_\epsilon\|_{\mathcal{H}_2} \leq \epsilon$. But $\|T(w)u_\epsilon\|_{\mathcal{H}_2}$ is continuous in w and hence $\limsup_{n\to\infty} \|T(z_n)^{-1}\|^{-1} \leq \epsilon$. We can argue similarly for the adjoint in the case that $\sigma_{\inf}(T(z)^*) = 0$. Since $\epsilon > 0$ was arbitrary and $\|T(z)^{-1}\|^{-1}$ is identically zero on $\Lambda(T)$, it follows that $\|T(z)^{-1}\|^{-1}$ is continuous.

It follows immediately from (2.10) that $\gamma_n(z,T) \geq \|T(z)^{-1}\|^{-1}$. Given $z \in \Omega$ and $\epsilon > 0$, let $u \in \mathcal{D}(T)$ of unit norm such that $\|T(z)u\|_{\mathcal{H}_2} \leq \sigma_{\inf}(T(z)) + \epsilon$. Since $\cup_{n\in\mathbb{N}}\mathcal{R}(\mathcal{P}_n)$ forms a core of $T(z)$, we may assume that $u = \mathcal{P}_n u$ for sufficiently large n. It follows that $\limsup_{n\to\infty} \sigma_{\inf}(T(z)\mathcal{P}_n^*) \leq \sigma_{\inf}(T(z)) + \epsilon$. We can argue in exactly the same manner for $T(z)^*$ and since $\epsilon > 0$ was arbitrary, we have $\lim_{n\to\infty} \gamma_n(z,T) = \|T(z)^{-1}\|^{-1}$. Since the sequences $\{\mathcal{P}_n\}$ and $\{\mathcal{Q}_n\}$ are increasing, the functions $\gamma_n(z,T)$ decrease monotonically in n. Since $\|T(z)^{-1}\|^{-1}$ is continuous, Dini's theorem implies that the convergence of $\gamma_n(z,T)$ is uniform on compact subsets of Ω.

The proof of (2.10) showed that $\sigma_{\inf}(T(z)) = \sigma_{\inf}(T(z)^*)$ for $z \in \rho(T)$. Continuity of $\sigma_{\inf}(T(z))$ and $\sigma_{\inf}(T(z)^*)$ shows that this equality extends to $z \in \partial\Lambda(T)$. The final part of the theorem statement now follows. ∎

Combining Theorems 2.2 and 2.3, we find that for any integer n, we have

$$\left\{z \in \Omega \,\middle|\, \gamma_n(z,T) < \epsilon\right\} \subset \Lambda_\epsilon(T). \tag{2.11}$$

Moreover, since the convergence of $\gamma_n(z,T)$ to $\|T(z)^{-1}\|^{-1}$ is locally uniform, these approximations converge to $\Lambda_\epsilon(T)$ as $n \to \infty$ without spectral pollution or spectral invisibility. This convergence is made precise in terms of the so-called Attouch–Wets topology, which generalizes the Hausdorff metric to closed (including unbounded) subsets of $\mathbb{C}$ [3]. There are generally two ways to make this a practical computation:

- If we have discretizations of the finite-rank operators $T(z)\mathcal{P}_n^*$ and $T(z)^*\mathcal{Q}_n^*$ that have finite lower bandwidths (or are well approximated by such matrices), we take rectangular truncations capturing the full range [30]. With respect to the appropriate norms, which can differ in the domain and range space, the smallest singular values of the resulting matrices are the same as those of $T(z)\mathcal{P}_n^*$ and $T(z)^*\mathcal{Q}_n^*$. Discretizations with finite lower bandwidths for the differential operators studied in this paper are provided by the ultraspherical spectral method [76].
- If we have discretizations of $\mathcal{P}_n T(z)^* T(z)\mathcal{P}_n^*$ and $\mathcal{Q}_n T(z) T(z)^* \mathcal{Q}_n^*$, then we can compute their smallest singular values and take square roots to compute γ_n [28].

The first method should be preferred over the second wherever possible since it avoids the loss of precision owing to the square root. In some situations, the second method seems unavoidable [25, 31]. It can be shown that it is not always possible to compute $\Lambda_\epsilon(T)$ by discretizing with square, finite sections $\mathcal{P}_n T \mathcal{P}_n^*$ of T [20]. One must be careful if one wants to compute $\Lambda_\epsilon(T)$ by discretizing first.

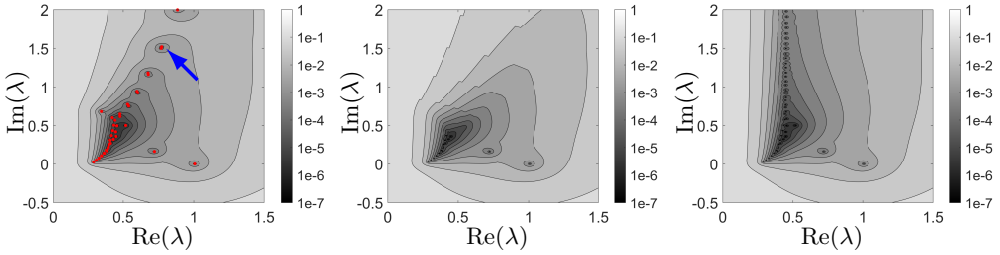

FIGURE 2.1. *The computed pseudospectra for the Orr–Sommerfeld NEP. Left: The pseudospectra is computed by first discretizing with $n = 64$ and then computing the pseudospectra of the matrix NEP with an appropriate weight matrix. The eigenvalues are shown as red dots and include a spurious branch labeled by a blue arrow. Middle: The computed pseudospectra using the functions γ_n from (2.9) for $n = 64$. These pseudospectral sets are guaranteed to be inside the pseudospectral sets of the infinite-dimensional problem and converge as $n \to \infty$. Right: The computed pseudospectra using γ_n for $n = 128$.*

2.3.1. Example: Orr–Sommerfeld. We consider the classical Orr– Sommerfeld equation as an example of the inclusion (2.11). When analyzing the temporal stability of fluid flows, this equation is a linear eigenvalue problem [77, 78]. However, if one considers spatial stability analysis, it becomes an NEP [82, Chapt. 7].

We consider a background plane Poiseuille flow $U(y) = 1 - y^2$ between two walls at $y = \pm 1$ with Reynolds number $R > 0$ and a fixed real perturbation frequency $\omega \in \mathbb{R}$. To define a NEP, we need the following two operators:

$$\mathcal{A}(\lambda)\phi = \left[\frac{1}{R}\mathcal{B}(\lambda)^2 + i\left(\lambda U(y) - \omega\right)\mathcal{B}(\lambda) + i\lambda U''(y)\right]\phi, \quad \mathcal{B}(\lambda)\phi \quad = -\frac{\mathrm{d}^2\phi}{\mathrm{d}y^2} + \lambda^2\phi.$$

The Orr–Sommerfeld operator is formally defined by $T(\lambda) = \mathcal{B}(\lambda)^{-1}\mathcal{A}(\lambda)$. Care is needed when defining the boundary conditions, domains, and appropriate spaces. Moreover, the spectral properties of the NEP depend on a choice of norms [90]. We equip $\mathcal{B}(\lambda)$ with Dirichlet boundary conditions $\psi(\pm 1) = 0$ and $T(\lambda)$ with boundary conditions $\psi(\pm 1) = 0$ and $\psi'(\pm 1) = 0$. The appropriate Hilbert space is $\mathcal{D}(\mathcal{B}(1))$ with the energy inner-product given by [34]

$$\langle \phi, \psi \rangle_E = \int_{-1}^{1} [\mathcal{B}(1)\phi]\overline{\psi}\,\mathrm{d}y = \int_{-1}^{1} \phi\overline{\psi} + \frac{\mathrm{d}\phi}{\mathrm{d}y}\frac{\mathrm{d}\overline{\psi}}{\mathrm{d}y}\,\mathrm{d}y. \tag{2.12}$$

We consider $\omega = 0.264002$ and $R = 5772.22$, corresponding to the critical neutral point for stability. In this case, $\Lambda(T)$ is discrete and $\partial\Lambda(T) = \Lambda(T)$. Hence, Theorem 2.3 tells us that the adjoint $T(\lambda)^*$ is not needed to compute $\Lambda_\epsilon(T)$. Other examples, such as Blasius boundary layer flow, have a continuous spectral component [45], and pseudospectra can also be computed using the functions γ_n for such problems.

This example goes under the name of `orr_sommerfeld` in the NLEVP collection, where it is discretized using a Chebyshev collocation method [88]. We compute the pseudospectra of these discretizations with appropriate weight matrices to take into account the norm induced by (2.12). For this problem, the pseudospectra of the discretized operators converge to the correct pseudospectra as the discretization size increases. However, deciding which regions of the computed pseudospectra are trustworthy can be challenging. We also compute the pseudospectra using the functions γ_n in (2.9) with a Legendre Galerkin spectral method and basis recombination to enforce the boundary conditions. For this basis, $\mathcal{A}\mathcal{P}_n^*$ and $\mathcal{B}\mathcal{P}_n^*$ are lower banded so we use rectangular truncation to compute $\gamma_n(z, T)$ and apply Theorem 2.3.

Figure 2.1 (left) shows pseudospectra of the discretized operators using $n = 64$ (NLEVP collection default) and Figure 2.1 (middle) shows γ_n for $n = 64$. There is a region where both pseudospectra agree. However, as $\mathrm{Im}(\lambda)$ increases, so do the differences between the pseudospectral sets. Due to (2.11), we can trust the output provided by γ_n and use it to discern which spectral regions of the Chebyshev collocation method have converged. Figure 2.1 (right) shows pseudospectra computed using γ_n for $n = 128$. This confirms our suspicions that there is a branch of spurious eigenvalues in the discretized NEP when $n = 64$. In subsection 4.3, we will see a striking example where pseudospectra of the discretized operators do not converge.

3. Stability and convergence analysis of infBeyn. We now obtain pseudospectral set inclusions for InfBeyn (see Algorithm 2.1) using Keldysh's theorem. InfBeyn computes the eigenvalues of the NEP inside the contour Γ via the pencil

$$\tilde{C}(z) = \tilde{\mathcal{U}}^*(\tilde{A}_1 - z\tilde{A}_0)\tilde{V}_0, \tag{3.1}$$

where $\tilde{A}_0 = \tilde{\mathcal{U}}\tilde{\Sigma}_0\tilde{V}_0^*$ is the SVD of $\tilde{A}_0$. Here, $\tilde{A}_0$ and $\tilde{A}_1$ are the approximations of A_0 and A_1, respectively, computed by InfBeyn via a quadrature rule and truncated singular value decomposition (see (2.7)).

We proceed in two steps. First, we relate $\tilde{C}$ to the following pencil:

$$C(z) = (A_1 - zA_0)V_0, \tag{3.2}$$

which amounts to understanding the errors incurred by quadrature rules (see subsection 3.2). In (3.2), V_0 denotes the right singular vector matrix of A_0. The range of $C(z)$ lies in $\mathcal{H}_1$, whereas its domain is $\mathbb{C}^m$. Second, we relate C to T, which is about controlling the error of InfBeyn when performed with exact integration (see subsection 3.3). Similar pseudospectral set inclusions are known for the FEAST method for linear eigenvalue problems [54]; however, the analysis is more challenging for NEPs.

3.1. Setup. Suppose that Γ is a contour that does not intersect $\Lambda(T)$ and bounds a simply-connected region $\mathrm{int}(\Gamma)$ containing eigenvalues $\lambda_1, \ldots, \lambda_s$ with total algebraic multiplicity m. If f is a holomorphic function on a neighborhood of $\mathrm{int}(\Gamma)$, then by the Cauchy integral formula, we have

$$\frac{1}{2\pi i}\int_\Gamma f(z)T(z)^{-1}\,\mathrm{d}z = Vf(J)W^*,$$

where J is a block Jordan matrix and V are W are the generalized right and left eigenvectors of T in Theorem 2.1. We assume that the quadrature rule used by InfBeyn is accurate in the sense that our approximations $\tilde{A}_j$ to A_j satisfy

$$\|A_j - \tilde{A}_j\| \le \epsilon, \qquad j = 1, 2, \tag{3.3}$$

where $\epsilon > 0$. Recall that A_0, A_1, $\tilde{A}_0$ and $\tilde{A}_1$ are of rank m (see subsection 2.2). Throughout the analysis, we also assume that $VW^*\mathcal{G}V_0$ is of rank m.

3.2. Controlling the errors incurred by quadrature rules. We begin by controlling how the errors in InfBeyn's quadrature rules perturb the spectral properties of its linear pencils, i.e., controlling the difference between $\tilde{C}$ (see (3.1)) and C (see (3.2)). These pencils map to different spaces, so we bound the difference between $\sigma_{\mathrm{inf}}(C)$ and $\sigma_{\mathrm{inf}}(\tilde{C})$, which directly bounds the differences in pseudospectra. Since $\tilde{\mathcal{U}}$ and $\tilde{V}_0$ have orthonormal columns and $\tilde{C}(z)$ is of rank at most m,

$$\sigma_{\mathrm{inf}}(\tilde{C}(z)) = \sigma_m(\tilde{C}(z)) = \sigma_m\left(\tilde{\mathcal{U}}(\tilde{\mathcal{U}}^*\tilde{A}_1\tilde{V}_0 - z\tilde{\mathcal{U}}^*\tilde{A}_0\tilde{V}_0)\tilde{V}_0^*\right) = \sigma_m(\tilde{\mathcal{U}}\tilde{\mathcal{U}}^*\tilde{A}_1\tilde{V}_0\tilde{V}_0^* - z\tilde{A}_0).$$

The last equality uses that $\tilde{\mathcal{U}}\tilde{\mathcal{U}}^*$ and $\tilde{V}_0\tilde{V}_0^*$ act as the identity on the column and row spaces of $\tilde{A}_0$, respectively. Similarly, $\sigma_{\inf}(C(z)) = \sigma_m(\mathcal{U}\mathcal{U}^* A_1 V_0 V_0^* - zA_0)$. Hence,

$$\left|\sigma_{\inf}(\tilde{C}(z)) - \sigma_{\inf}(C(z))\right| \leq \|P_1 A_1 P_2 - \tilde{P}_1\tilde{A}_1\tilde{P}_2\| + |z|\|A_0 - \tilde{A}_0\|,$$

where $P_1 = \mathcal{U}\mathcal{U}^*$, $\tilde{P}_1 = \tilde{\mathcal{U}}\tilde{\mathcal{U}}^*$, $P_2 = V_0V_0^*$, and $\tilde{P}_2 = \tilde{V}_0\tilde{V}_0^*$. By the triangle inequality,

$$\|P_1 A_1 P_2 - \tilde{P}_1\tilde{A}_1\tilde{P}_2\| \leq \|A_1\|(\|P_1 - \tilde{P}_1\| + \|P_2 - \tilde{P}_2\|) + \|A_1 - \tilde{A}_1\|.$$

Since A_0 and $\tilde{A}_0$ have the same rank, we know that [19]:

$$\|P_1 - \tilde{P}_1\| + \|P_2 - \tilde{P}_2\| \leq 2\min\{\|A_0^\dagger\|, \|\tilde{A}_0^\dagger\|\}\|A_0 - \tilde{A}_0\| \leq 2\|A_0^\dagger\|\|A_0 - \tilde{A}_0\|,$$

where $A_0^\dagger$ denotes the pseudoinverse of A_0. From (3.3), we conclude that

$$\left|\sigma_{\inf}(\tilde{C}(z)) - \sigma_{\inf}(C(z))\right| \leq (2\|A_0^\dagger\|\|A_1\| + |z| + 1)\epsilon. \tag{3.4}$$

One can interpret (3.4) as telling us that the pseudospectral sets of $C(z)$ and $\tilde{C}(z)$ are close. Precisely how close is determined by the errors incurred when computing A_0 and A_1 with a quadrature rule, i.e., $\|A_0 - \tilde{A}_0\|$ and $\|A_1 - \tilde{A}_1\|$, as well as the quantity $\|A_0^\dagger\|\|A_1\|$ that is related to the intrinsic spectral properties of T (see (3.8)).

3.3. Stability analysis with exact integration. We now relate the pseudospectral sets of C and T. Combined with (3.4), the following bounds will allow us to prove pseudospectral set inclusions between $\tilde{C}$ (the pencil used to compute eigenvalues in InfBeyn) and T (the original NEP) inside Γ.

THEOREM 3.1. *Assume the same conditions for T as in subsection 2.1 and the setup in subsection 3.1. For sufficiently small $\delta > 0$, the following pseudospectral set inclusions hold inside Γ:*

$$\Lambda_{\delta_1}(T) \cap \mathrm{int}(\Gamma) \subset \Lambda_\delta(C) \cap \mathrm{int}(\Gamma) \subset \Lambda_{\delta_2}(T) \cap \mathrm{int}(\Gamma), \tag{3.5}$$

where

$$\delta_1 = \frac{\delta}{\|VW^*\|\|VW^*\mathcal{G}\| + M\delta}, \qquad \delta_2 = \frac{\delta}{\sigma_m(VW^*)\sigma_m(VW^*\mathcal{G}) - M\delta}.$$

Here, V and W are the matrices of generalized eigenvectors, $\mathcal{G}$ is the random quasimatrix in subsection 2.2 and $M = \sup_{z\in\mathrm{int}(\Gamma)}\|R(z)\|$.

Proof. We first prove the right side of the inclusion. Let $z \in \mathrm{int}(\Gamma)$ such that $\sigma_{\inf}(C(z)) < \delta$ and define $L_1 = (VW^*)^\dagger$. If $z \in \Lambda(T)$, then (3.5) immediately holds, and there is nothing to prove. If $T(z)^{-1}$ exists, Keldysh's theorem implies that

$$\begin{aligned} T(z)^{-1}L_1C(z) &= [V(zI - J)^{-1}W^* + R(z)](VW^*)^\dagger V(J - zI)W^*\mathcal{G}V_0 \\ &= -VW^*\mathcal{G}V_0 + R(z)L_1C(z), \end{aligned} \tag{3.6}$$

where we have used $C(z) = V(J - zI)W^*\mathcal{G}V_0$. Since $\sigma_{\inf}(C(z)) < \delta$, there exists a unit-norm $x \in \mathbb{C}^m$ with $\|C(z)x\| < \delta$. Furthermore, $u = L_1C(z)x \neq 0$; otherwise, $VW^*\mathcal{G}V_0x = 0$ and $VW^*\mathcal{G}V_0$ would not be of rank m. We also have that

$$\|u\| \leq \|L_1\|\|C(z)x\| < \delta/\sigma_m(VW^*).$$

This means that

$$\left\|T(z)^{-1}\frac{u}{\|u\|}\right\| \geq \frac{\|VW^*\mathcal{G}V_0x\|}{\|u\|} - M > \frac{\sigma_m(VW^*)\sigma_m(VW^*\mathcal{G})}{\delta} - M,$$

where $M = \sup_{z\in\text{int}(\Gamma)} \|R(z)\|$. It follows that if δ is sufficiently small so that $M\delta < \sigma_m(VW^*)\sigma_m(VW^*\mathcal{G})$, then $z \in \Lambda_{\delta_2}(T)$. Hence, $\Lambda_\delta(C) \cap \text{int}(\Gamma) \subset \Lambda_{\delta_2}(T) \cap \text{int}(\Gamma)$.

For the other inclusion, let $z \in \text{int}(\Gamma)$ with $\|T(z)^{-1}\| > 1/\delta_1$, where $\delta_1 = \delta/(\|VW^*\|\|VW^*\mathcal{G}\| + M\delta)$, and define $L_2 = (VW^*\mathcal{G}V_0)^\dagger$. If $\sigma_{\inf}(C(z)) = 0$, there is nothing to prove. Hence, assume that $\sigma_{\inf}(C(z)) > 0$, so that $T(z)^{-1}$ exists and

$$C(z)L_2[T(z)^{-1} - R(z)] = V(J - zI)W^*\mathcal{G}V_0(W^*\mathcal{G}V_0)^\dagger V^\dagger V(z - J)^{-1}W^* = -VW^*.$$

There exists u of unit norm such that $\|T(z)^{-1}u\| > 1/\delta_1$. Provided that δ_1 is sufficiently small so that $\delta_1 < 1/M$, we know that

$$\|T(z)^{-1}u - R(z)u\| > 1/\delta_1 - M > 0.$$

Since $\left(T(z)^{-1} - R(z)\right)u = V(z - J)^{-1}W^*u$ lies in the range of V, it follows that $x = L_2\left(T(z)^{-1} - R(z)\right)u$ satisfies the following inequality:

$$\|x\| \geq \sigma_m(L_2)\|\left(T(z)^{-1} - R(z)\right)u\| > \frac{1/\delta_1 - M}{\|VW^*\mathcal{G}V_0\|} = \frac{1/\delta_1 - M}{\|VW^*\mathcal{G}\|}.$$

This means we have

$$\left\|C(z)\frac{x}{\|x\|}\right\| = \frac{\|VW^*u\|}{\|x\|} < \frac{\|VW^*\mathcal{G}\|}{1/\delta_1 - M}\|VW^*u\| \leq \frac{\|VW^*\mathcal{G}\|\|VW^*\|}{1/\delta_1 - M} = \delta.$$

Hence, we conclude that $\Lambda_{\delta_1}(T) \cap \text{int}(\Gamma) \subset \Lambda_\delta(C) \cap \text{int}(\Gamma)$, finishing the proof. ∎

Theorem 3.1 tells us that when InfBeyn is performed with exact integration, the constructed pencil is very reasonable for computing the eigenvalues of T provided that VW^* and $VW^*\mathcal{G}$ are well-conditioned, and M is not too large.

3.4. Pseudospectral set inclusions and interpretation. Combining (3.4) and Theorem 3.1, we conclude that

$$\Lambda_{\delta_-}(T) \cap \text{int}(\Gamma) \subset \Lambda_\delta(\tilde{C}) \cap \text{int}(\Gamma) \subset \Lambda_{\delta_+}(T) \cap \text{int}(\Gamma), \tag{3.7}$$

where $\gamma_\pm = \delta \pm (2\|A_0^\dagger\|\|A_1\| + 1 + \sup_{z\in\text{int}(\Gamma)}|z|)\epsilon$ and

$$\delta_- = \frac{\gamma_-}{\|VW^*\|\|VW^*\mathcal{G}\| + M\gamma_-}, \quad \delta_+ = \frac{\gamma_+}{\sigma_m(VW^*)\sigma_m(VW^*\mathcal{G}) - M\gamma_+}.$$

Since InfBeyn uses the pencil $\tilde{C}$ to compute the eigenvalues of T inside Ω, (3.7) tells us that InfBeyn robustly computes the eigenvalues of T provided that the following conditions hold: (1) VW^* is well-conditioned, (2) $VW^*\mathcal{G}$ is well-conditioned,[6] (3) the holomorphic remainder is not too large inside int(Γ), i.e., M is not too big, (4) $\|A_0^\dagger\|\|A_1\|$ is relatively small, and (5) ϵ is small.

The NEP intrinsically determines condition (1). Once condition (1) holds, condition (2) follows in practice, provided that the sketching performed by InfBeyn is adequate at capturing the range of $\mathcal{A}_0$ and $\mathcal{A}_1$. Condition (3) measures the regularity of T inside Ω, while (4) is about the regularity of the pencil C if no quadrature error

[6] It can be shown that for $p = 5$ we have $\sigma_m(VW^*\mathcal{G}) \geq 50\sigma_m(VW^*)\text{Trace}((W^*KW)^{-1})$ with probability $> 99.999\%$ (see [14, Lem. 3] with $t = 10$). Here, K is the covariance kernel in $\mathcal{GP}(0, K)$ used to randomly generate the columns of $\mathcal{G}$. Moreover, for $p = 5$, $\|VW^*\mathcal{G}\| \leq 9(m+5)\|VW^*\|\text{Trace}(K)$ with probability $> 99.999\%$ (see [14, Lem. 4] with $s = 3$), where Trace(K) is the sum of the eigenvalues of K. In practice, $VW^*\mathcal{G}$ is well-conditioned when $p \geq 5$, VW^* is well-conditioned, and the covariance kernel in $\mathcal{GP}(0, K)$ is reasonably selected.

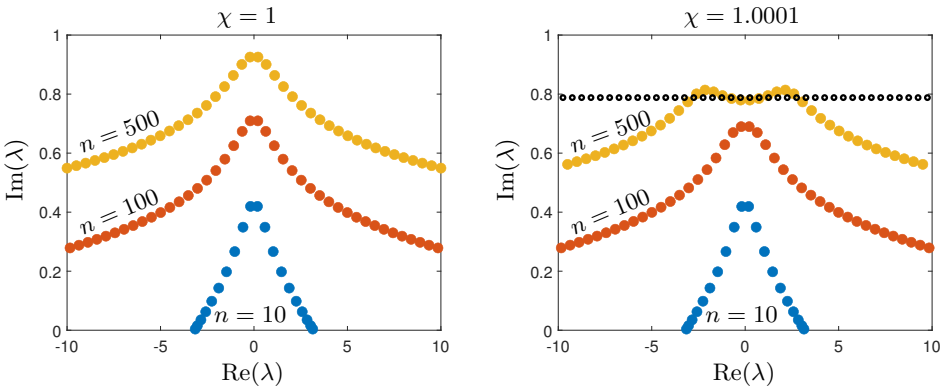

FIGURE 4.1. *Computed eigenvalues for the discretized acoustic wave 1D example labeled as* `acoustic_wave_1d` *in the NLEVP collection with discretization size* $n = 10$ *(blue),* $n = 100$ *(red), and* $n = 500$ *(yellow). Left: The spectrum of the infinite-dimensional problem is empty, and all the computed eigenvalues are spurious. Right: The computed eigenvalues are correctly converging as* $n \to \infty$ *to the spectra of the infinite-dimensional problem (black dots), but the convergence is slow.*

is incurred. By Keldysh's expansion, we see that

$$\|A_0^\dagger\|\|A_1\| \le \sigma_m(VW^*\mathcal{G})\|VJW^*\mathcal{G}\| \le \sigma_m(VW^*\mathcal{G})\|VJW^*\|\|\mathcal{G}\|. \tag{3.8}$$

Again, one expects that (4) holds, provided that the sketching performed by InfBeyn is adequate. Finally, (5) suggests that InfBeyn's quadrature rules should be relatively accurate. In short, (3.7) tells us that InfBeyn is a robust method for computing the eigenvalues of an NEP inside a compact region of the complex plane.

4. Six NEPs with unsettling discretization issues. It turns out that 25 of the 52 matrix NEPs from the NLEVP collection are derived by discretizing an infinite-dimensional NEP. To showcase the unsettling discretization effects, we take six examples from the NLEVP collection and show how discretization has modified, destabilized, and destroyed spectra. To ensure we report problems caused by discretization alone, we have verified the computed eigenvalues of the discretized NEPs with extended precision. The eigenvalues computed using InfBeyn are verified by computing infinite-dimensional residuals, similar in spirit to subsection 2.3.

4.1. Example 1: One-dimensional acoustic wave. This is a differential boundary eigenvalue problem posed on $L^2([0,1])$ that takes the form

$$\frac{\mathrm{d}^2 p}{\mathrm{d}x^2} + 4\pi^2\lambda^2 p = 0, \qquad p(0) = 0, \quad \chi p'(1) + 2\pi i\lambda p(1) = 0. \tag{4.1}$$

Here, p is the acoustic pressure, λ is the frequency, and χ is the (possibly complex) impedance [18]. The eigenvalues correspond to the resonant frequencies of the system and can be calculated explicitly (for values of χ for which $\tan^{-1}(i\chi)$ is finite) as:

$$\lambda_k = \tan^{-1}(i\chi)/(2\pi) + k/2, \qquad k \in \mathbb{Z}. \tag{4.2}$$

This problem goes under the name of `acoustic_wave_1d` and is the first problem listed in the NLEVP collection. It is commonly discretized using finite element method (FEMs) [50] to form a quadratic matrix NEP.

We first consider the default value $\chi = 1$, which is also a value of χ that makes

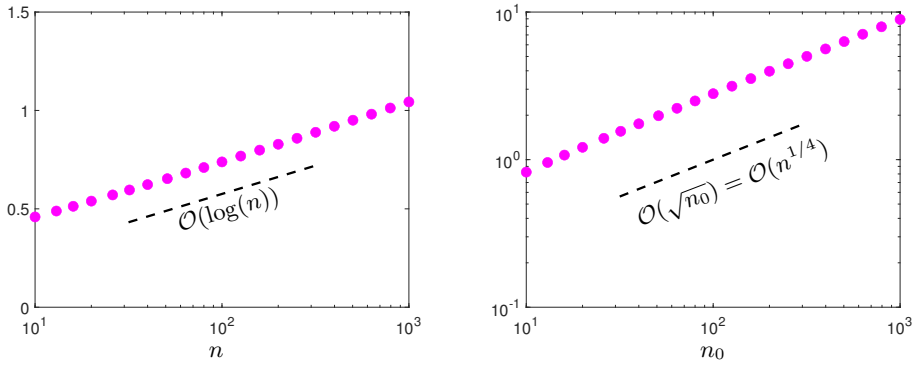

FIGURE 4.2. *The minimum absolute value of the spurious eigenvalues as a function of n. Left: The acoustic wave 1D example. Right: The acoustic wave 2D example, where the true discretization size is $n = n_0(n_0 - 1)$.*

$\tan^{-1}(i\chi)$ in (4.2) infinite.[7] We compute the eigenvalues of the discretized problem for three discretization sizes $n = 10$, 100, and 500 (see Figure 4.1 (left)). We compute these eigenvalues using the `polyeig` command in MATLAB. One can easily show that the spectrum of (4.1) is empty for $\chi = 1$. Hence, all these computed eigenvalues are spurious and can be regarded as meaningless for the original problem in (4.1). Figure 4.2 (left) shows the minimum absolute value of the eigenvalues as a function of n. The eigenvalues march off to infinity, but incredibly slowly.

We repeat the experiment with the value $\chi = 1.0001$ so that (4.1) no longer has an empty spectrum. Again, we discretize (4.1) using FEMs [50] with $n = 10$, 100, and 500 and compute the eigenvalues of the matrix NEP using `polyeig`. The computed eigenvalues are now converging as $n \to \infty$; however, the rate is very slow (see Figure 4.1 (right)). This example shows that even when the eigenvalues of the discretization are converging, it can be computationally prohibitive if the rate is slow. Moreover, it is easy to be misled, even when comparing different discretization sizes [16]. Hence, methods that verify computations (e.g., using the infinite-dimensional pseudospectra techniques of subsection 2.3 to verify the output of InfBeyn) are very useful.

4.2. Example 2: Two-dimensional acoustic wave. In the NLEVP collection, a 2D acoustic wave example goes under the name of `acoustic_wave_2d` and is discretized using FEMs. The NEP is posed on $L^2([0,1]^2)$ and given by

$$\frac{\partial^2 p}{\partial x^2} + \frac{\partial^2 p}{\partial y^2} + 4\pi^2\lambda^2 p = 0$$
$$p(0,y) = p(x,0) = p(x,1) = 0, \quad \chi\frac{\partial p}{\partial x}(1,y) + 2\pi i\lambda p(1,y) = 0, \tag{4.3}$$

with the same meaning of the parameters as in (4.1).

We first select $\chi = 1$. For this value of χ, the spectrum of (4.3) is non-empty, unlike the 1D case. However, (4.3) has no eigenvalues in the region $[-10, 10] \times [0.6, 4]$ in the complex plane, which can be proved using an argument principle. Despite this, the matrix NEPs for $n = 56$, 240, and 506 have spurious eigenvalues in that region

[7] More precisely, we consider the operator $T(\lambda) : H^2(0,1) \to L^2(0,1) \times \mathbb{C}^2$ given by $T(\lambda)p = (-p'' - (2\pi\lambda/c)^2 p, p(0), \chi p'(1) + 2\pi i\lambda p(1))$. The operator $\lambda^2 T(1/\lambda)$ has essential spectra at $\lambda = 0$. Hence, this problem has essential spectra (not eigenvalues) at infinity for any χ.

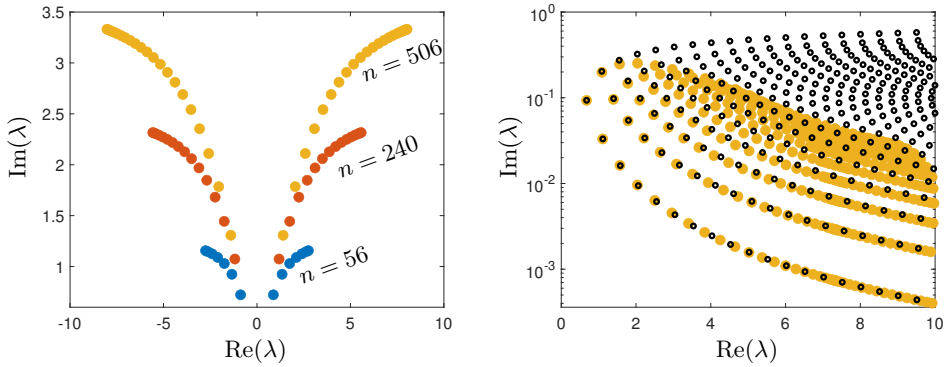

FIGURE 4.3. *The spectra of the acoustic wave 2D example for $\chi = 1$. Left: Eigenvalues of the discretized problem,* `acoustic_wave_2d`*, for discretization sizes $n = 56$, 240, and 506. The discretization sizes are constrained to be of the form $n = n_0(n_0 - 1)$. There are no eigenvalues of (4.3) in this region. Right: A region in the complex plane close to the real axis that does contain eigenvalues of (4.3). These are shown as black dots and are computed using InfBeyn, where we separate the problem into a family of one-dimensional problems. The yellow dots are eigenvalues of the discrete problem for $n = 506$, showing convergence to a proportion of them. We only show a region in the right-half plane because the spectrum of the infinite-dimensional NEP and eigenvalues of the discretization are symmetric about the imaginary axis.*

caused by the discretization (see Figure 4.3 (left)). Figure 4.2 (right) shows how severe this is. The spurious eigenvalues only exit the disc of radius 10 after a discretization size in excess of 10^6. There is a region close to the real axis in the complex plane for which the discretizations do correctly approximate the spectra (see Figure 4.3 (right)). Determining which regions the discretization will have spurious eigenvalues and which regions the computed eigenvalues can be trusted seems challenging. To give an idea of how hard this is, the location of spectral pollution for linear eigenvalue problems has only very recently been characterized in any sense of generality [11]. In contrast, InfBeyn correctly returns no eigenvalues in the region $[-10, 10] \times [0.6, 4]$ in the complex plane and accurately computes the eigenvalues close to the real axis. In summary, the discretizations exhibit spurious eigenvalues in one region and slow convergence in another. This example is a cause for concern because the two regions are relatively close together in the complex plane, making it challenging to identify spectral pollution after discretization.

When $\chi \notin (-\infty, -1] \cup [1, \infty)$, a subset of the spectrum is given by an infinite number of simple eigenvalues that obey the following asymptotic formula:

$$\lambda_k \sim \text{sign}\left[\text{Re}\left(i\sqrt{\frac{1}{\chi^2 - 1}}\right)\right] k/(2\sqrt{1 - 1/\chi^2}), \qquad k \to \infty,$$

where the sign function is required to take care of branch cuts. We now take $\chi = 0.8$, and for this value of χ, the eigenvalues of (4.3) that obey the above asymptotic formula are purely imaginary. Figure 4.4 shows the approximation of these eigenvalues using the discrete problem with different discretization sizes. Again, the eigenvalues of the infinite-dimensional problem are shown as black circles and computed using InfBeyn. The eigenvalues of the discrete problem are symmetric across the imaginary axis. As the kth pair approaches the imaginary axis, they collide, and the pair splits. One eigenvalue converges to λ_k, while the other shoots off to infinity. In other words, the discrete problem overestimates the actual multiplicity.

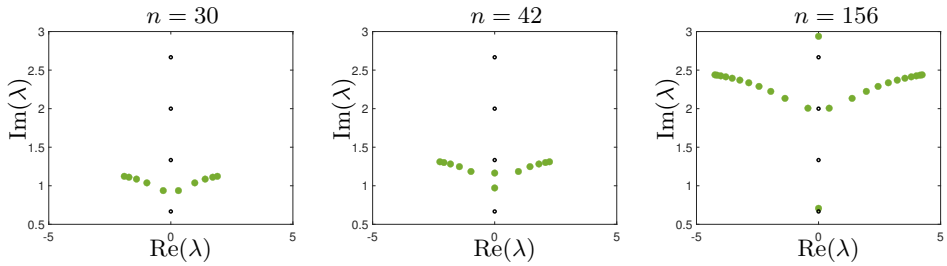

FIGURE 4.4. *As the discretization size increases, we observe the eigenvalues of the discretization (green dots) collide onto the imaginary axis, and a few converge to the eigenvalues of the infinite-dimensional problem (black dots). The eigenvalues of the discretization are potentially misleading because the eigenvalues of the infinite-dimensional problem are simple. Still, it appears that two eigenvalues of the discretization are converging to each eigenvalue.*

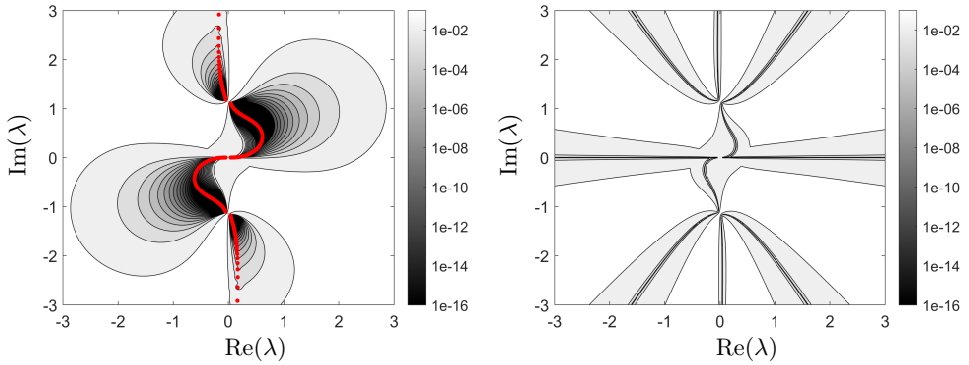

FIGURE 4.5. *The computed pseudospectra of the butterfly NEP. Left: The pseudospectra of the discretized pencil using matrices of size $n = 500$. The eigenvalues are shown as red dots and converge to the union of four arcs as $n \to \infty$. Right: The pseudospectra computed using the functions γ_n from (2.9) and an adaptive truncation size. These pseudospectra are guaranteed to be inside the pseudospectra of the infinite-dimensional problem and converge as $n \to \infty$.*

4.3. Example 3: Butterfly. As our next example, we further show the importance of verification of approximated pseudospectra in (2.11) and that our techniques are not limited to differential operators. We consider the NEP called `butterfly` from the NLEVP collection, which is a rational NEP constructed from truncations of bilateral shift operators on $\ell^2(\mathbb{Z})$ [71]. The pencil depends on a vector $c \in \mathbb{C}^{10}$ which we take as $c = [0.2i, 0, 1.3, 0, 0.1, 0, 1, 0, 0, 0]$.

Figure 4.5 (left) shows the eigenvalues and pseudospectra of the discretized problem using matrix sizes $n = 500$. The eigenvalues appear to converge to four arcs in the complex plane as $n \to \infty$. In the right of Figure 4.5, we show pseudospectra computed using the functions γ_n from (2.9). The operators are infinite banded matrices acting on $l^2(\mathbb{Z})$; hence, it is straightforward to compute γ_n directly using rectangular truncations. We use a λ-adaptive truncation size to ensure convergence of the plot. The plots show that the discretized operator suffers from spectral pollution, invisibility, and destabilization. For this particular example, changing the discretization to circulant matrices approximating the shift is better. However, in general, such a procedure is not guaranteed to circumvent the issues caused by discretization.

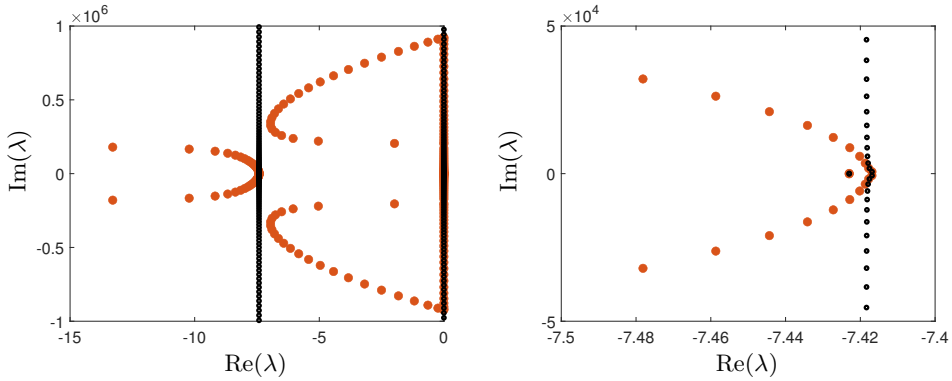

FIGURE 4.6. *Computed eigenvalues of discretization (red dots) compared to the eigenvalues computed from InfBeyn (black dots). Left: Eigenvalues in the region* $[-15,0]\times[-10^6,10^6]$. *Right: A magnified picture of the eigenvalues in the region* $[-7.5,-7.4]\times[-5\times10^4,5\times10^4]$. *The eigenvalues of the discretized NEP show significant errors.*

4.4. Example 4: Damped beam. We now consider the NEP that goes by the name `damped_beam` in the NLEVP collection. It is given by

$$\frac{\mathrm{d}^4 v}{\mathrm{d}x^4}(x)-\alpha_0\lambda^2 v(x)=\beta\lambda v(x)\delta(x-1/2),\quad v(0)=\frac{\mathrm{d}^2 v}{\mathrm{d}x^2}(0)=v(1)=\frac{\mathrm{d}^2 v}{\mathrm{d}x^2}(1)=0, \tag{4.4}$$

where $\alpha_0,\beta<0$ are fixed physical constants and v represents the transverse displacement of the beam. We take the default NLEVP parameter values of $\alpha_0=-0.018486857142857$ and $\beta=-0.137142857142857$. The delta function $\delta(\cdot)$ in (4.4) is interpreted as continuity of v, v', and v'' at $x=1/2$, but with a jump in v''', i.e.,

$$\lim_{\epsilon\downarrow 0}\left[\frac{\mathrm{d}^3 v}{\mathrm{d}x^3}(1/2+\epsilon)-\frac{\mathrm{d}^3 v}{\mathrm{d}x^3}(1/2-\epsilon)\right]=\beta\lambda v(1/2).$$

The NEP is a quadratic eigenvalue problem that arises in the vibration analysis of a beam supported at both ends and damped in the middle [52].

We discretize (4.4) using a finite element method with cubic Hermite polynomials as the interpolation shape functions [32]. There are two groups of eigenvalues for (4.4). The first group is purely imaginary and given by the following formula:

$$\lambda_k^{(1,\pm)}=\pm 4\pi^2 k^2 i/\sqrt{-\alpha_0},\quad k\geq 0,$$

with corresponding eigenfunctions that vanish at $x=1/2$. The second group has the following asymptotic formula:

$$\lambda_k^{(2,\pm)}=\frac{4}{\sqrt{\alpha_0}}\left[\pm\left(k\pi-\frac{\pi}{2}\right)i+\frac{\beta}{8k\pi\sqrt{-\alpha_0}}\right]^2+\mathcal{O}\left(\frac{1}{k}\right),\qquad k\to\infty. \tag{4.5}$$

Asymptotic formulas benefit contour-based methods as they inform us where to center contours. In addition, if the asymptotic formula comes with an explicit error estimate, we can choose the contour size. The asymptotic formula in (4.5) allows us to compute $\lambda_k^{(2,\pm)}$ for large k using InfBeyn with a circular contour of radius 1 centered at (4.5). An alternative to asymptotics is localization theorems for NEPs [8], which are also very useful for contour methods.

Figure 4.6 shows the eigenvalues of the discretized problem for the discretization size $n=100$ and the eigenvalues computed using InfBeyn. Comparing InfBeyn's

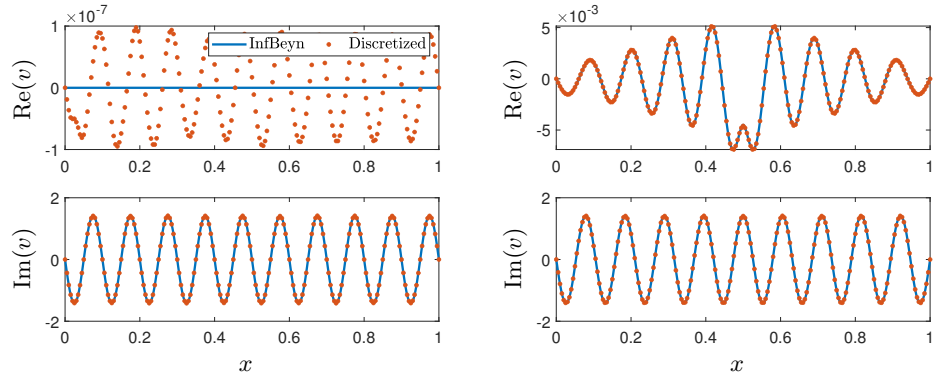

FIGURE 4.7. *The real (top row) and imaginary (bottom row) of the eigenfunctions corresponding to* $\lambda_{10}^{(1,+)}$ *(left) and* $\lambda_{10}^{(2,+)}$ *(right). Surprisingly, the eigenfunctions are well-resolved by the discrete NEP while the corresponding eigenvalues* $\lambda_{10}^{(1,+)}$ *and* $\lambda_{10}^{(2,+)}$ *are not.*

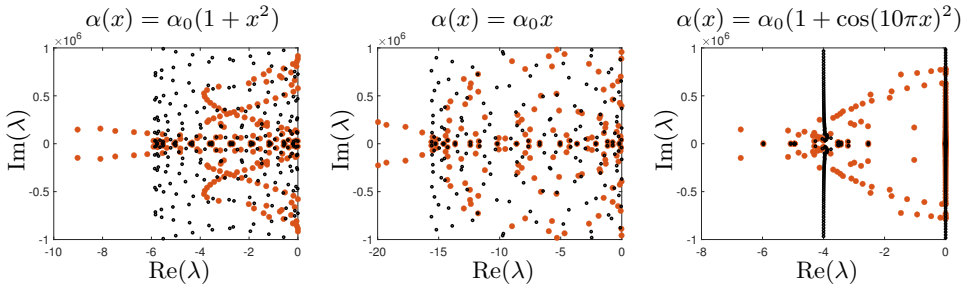

FIGURE 4.8. *Same as Figure 4.6 but with the displayed variable coefficient* $\alpha(x)$ *replacing* α_0 *in (4.4).*

approximation of $\lambda_k^{(2,+)}$ for $1 \le k \le 100$ and the first four terms of the asymptotics shows that InfBeyn has computed all of the eigenvalues in Figure 4.7 to relative error smaller than 10^{-12}. The discretization does a good job of approximating the real part of the first group of eigenvalues $\{\lambda_k^{(1,\pm)}\}$, but only a handful of the eigenvalues are accurate due to errors in the imaginary part. Surprisingly, we observe that the corresponding eigenfunctions are well-resolved by the discretization. For example, Figure 4.7 shows the approximation of the eigenfunctions corresponding to $\lambda_{10}^{(1,+)}$ and $\lambda_{10}^{(2,+)}$. The $L^2([0,1])$ subspace angle between the approximate eigenfunction and the true eigenfunction (computed using InfBeyn) are approximately 10^{-3}. However, the error in the approximation of $\lambda_{10}^{(1,+)}$ and $\lambda_{10}^{(2,+)}$, are 48.1040 and 35.5109, respectively. Therefore, resolving the eigenfunctions is insufficient for accurately computing the corresponding eigenvalues. We find this extremely unsettling. Figure 4.8 shows the computed eigenvalues when we replace α_0 (4.4) by a variable coefficient $\alpha(x)$.[8] The regions in the complex plane where the computed eigenvalues are reliable depend non-trivially on the coefficient.

[8]For NEPs consisting of coupled PDEs with constant coefficients, we can sometimes solve for the eigenvalue-dependent solution on each domain and reduce the problem to a finite-dimensional NEP relating the boundary values [2]. This can be done for (4.4) when all the coefficients are constant but cannot generally be done for variable coefficients.

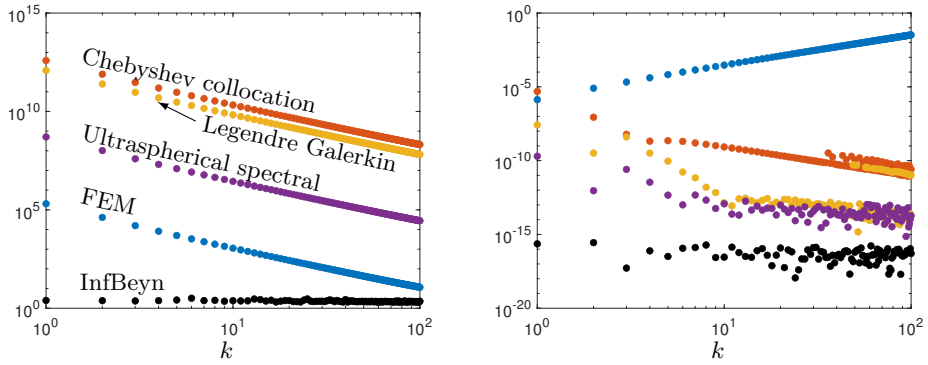

FIGURE 4.9. *A comparison of four discretization methods and InfBeyn for (4.6). Left: InfBeyn is stable. In contrast, a discretization method can construct an NEP with severely ill-conditioned eigenvalues. Right: The relative accuracy of the computed eigenvalues.*

4.5. Example 5: A loaded string. Next, we look at another NEP in the NLEVP collection named `loaded_string`. The NEP is given by

$$-\frac{\mathrm{d}^2u}{\mathrm{d}x^2} = \lambda u, \qquad u(0) = 0, \quad \frac{\mathrm{d}u}{\mathrm{d}x}(1) + \frac{\lambda\kappa M}{\lambda - \kappa}u(1) = 0. \tag{4.6}$$

It models the vibrations of a string with a mass load M attached to an elastic spring with stiffness κ [84]. We use the default parameters $M = \kappa = 1$. The eigenvalues of physical interest lie in the interval $(\kappa, \infty) \subset \mathbb{R}$ and are solutions of

$$\cos\left(\sqrt{\lambda}\right) + \frac{\sqrt{\lambda}\kappa M}{\lambda - \kappa}\sin\left(\sqrt{\lambda}\right) = 0. \tag{4.7}$$

Since the infinite-dimensional NEP has a Rayleigh quotient that increases monotonically with the spectral parameter, one can show that a linear FEM constructs a discrete NEP whose eigenvalues converge to the spectrum of (4.6) without spectral pollution or missing eigenvalues [83]. However, discretization can still introduce severe ill-conditioning, potentially (but not necessarily) causing inaccurate computed eigenvalues in floating-point arithmetic.

We consider four methods of discretization and compare them with InfBeyn. The first discretization uses finite elements as proposed in [84], the second uses a Chebyshev collocation method [35], the third uses a standard Galerkin method using Legendre polynomials, and the fourth uses the ultraspherical spectral method [76]. To calculate the accuracy of each discretization method, we compute solutions to (4.7) using Newton's method with initial guesses provided by the asymptotic formula $\lambda_k \sim (k - 1/2)^2\pi^2$ as $k \to \infty$. This asymptotic formula also guides us in selecting the centers of the contours for InfBeyn.

Figure 4.9 (left) shows the relative condition numbers of the first 100 eigenvalues of the resulting discrete NEPs (see [47, Thm. 2.20] for the condition number formula) for 500×500 discretizations. We also show the corresponding condition numbers for InfBeyn. We see the stability of InfBeyn, as predicted by our analysis in section 3. While the condition numbers are interesting, they give little insight into the final accuracy of the computed eigenvalues (see Figure 4.9 (right)), which may be because floating-point rounding errors are causing highly structured perturbations.

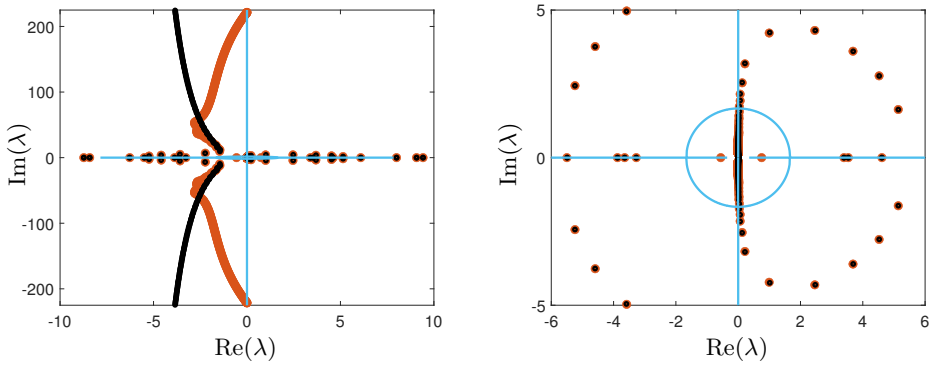

FIGURE 4.10. *Spectra of the planar waveguide problem in the λ plane. Left: The eigenvalues of the discretized planar waveguide problem are shown in red. The eigenvalues computed by InfBeyn are shown as black circles and verified using infinite-dimensional residuals. Right: A magnified region near $\lambda = 0$. The discretized problem has spurious modes, and several branches of the modes collapse onto the essential spectrum of the underlying problem posed on $\mathbb{R}$ (shown in light blue).*

Moreover, the relative accuracy of the computed eigenvalues is also due to how fast the eigenvalues of the discretization converge.

4.6. Example 6: Planar waveguide. For our final example, we consider the NEP called `planar_waveguide` in the NLEVP collection. This NEP describes the propagation properties of electromagnetic waves in multilayered media, characterized by a refractive index η that varies in x-direction [86]. The original problem is a linear problem on the unbounded domain $\mathbb{R}$ that has both discrete and essential spectra [67].

More precisely, consider a material that consists of $J+1$ layers described by refractive indices $\eta_0, \ldots, \eta_J$ and the positions of the interfaces $x_1 = 0 < x_2 < \cdots < x_J = L$, so that $\eta(x) = \eta_0$ if $x < x_1$, $\eta(x) = \eta_j$ if $x_j < x < x_{j+1}$ and $\eta(x) = \eta_J$ if $x > x_J$. The truncated domain is $[x_1, x_J] = [0, L]$. For a frequency k, we define $\delta_\pm = k^2(\eta_0^2 \pm \eta_J^2)/2$. The NEP is given by

$$\begin{aligned} &\frac{\mathrm{d}^2\phi}{\mathrm{d}x^2}(x) + k^2[\eta^2(x) - \mu(\lambda)]\phi(x) = 0, \quad \mu(\lambda) = \frac{\delta_+}{k^2} + \frac{\delta_-}{8k^2\lambda^2} + \frac{\lambda^2}{k^2}, \\ &\frac{\mathrm{d}\phi}{\mathrm{d}x}(0) + \left(\frac{\delta_-}{2\lambda} - \lambda\right)\phi(0) = 0, \quad \frac{\mathrm{d}\phi}{\mathrm{d}x}(L) + \left(\frac{\delta_-}{2\lambda} + \lambda\right)\phi(L) = 0. \end{aligned} \tag{4.8}$$

We take the default parameters $J = 5$, $\eta_0 = 1.5, \eta_1 = 1.66, \eta_2 = 1.6, \eta_3 = 1.53, \eta_4 = 1.66, \eta_5 = 1.0$, $x_2 = 0.5, x_3 = 1.0, x_4 = 1.5, x_5 = 2.0$ and $k = 2\pi/0.6328$.

We discretize (4.8) using piecewise linear finite elements. Figure 4.10 shows the eigenvalues computed using finite elements and a discretization size of $n = 129$ (NLEVP's default value) and those computed using InfBeyn. We also show the essential spectrum of the linear problem on the unbounded domain, which is given by λ such that $\mu(\lambda) \in (-\infty, \max\{\eta_0^2, \eta_J^2\}]$.[9] The majority of the eigenvalues of the discretized NEP are inaccurate, and there are also spurious guided modes. Many modes have collapsed onto the essential spectrum of the linear eigenvalue problem posed on $\mathbb{R}$. This issue is common with discretized problems of this type [41, Fig. 3], and we

[9] To see this, one considers the altered linear problem on $\mathbb{R}$ with $\eta_1 = \cdots = \eta_J$, where the essential spectrum is $\mu(\lambda) \in (-\infty, \max\{\eta_0^2, \eta_J^2\}]$. One then shows that the resolvents of the altered problem differ from the original by a compact operator [59, p. 244].

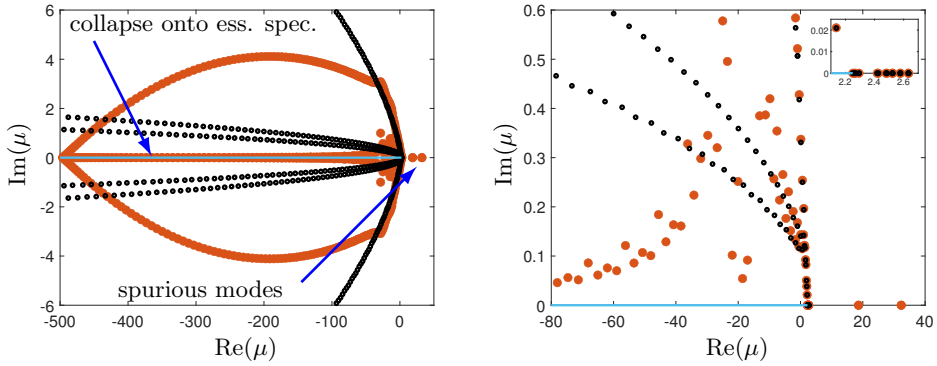

FIGURE 4.11. *Same as Figure 4.10 but in the $\mu(\lambda)$ plane. The essential spectrum of the underlying problem posed on $\mathbb{R}$ is the semi-infinite interval $\mu \in (-\infty, \max\{\eta_0^2, \eta_J^2\}]$.*

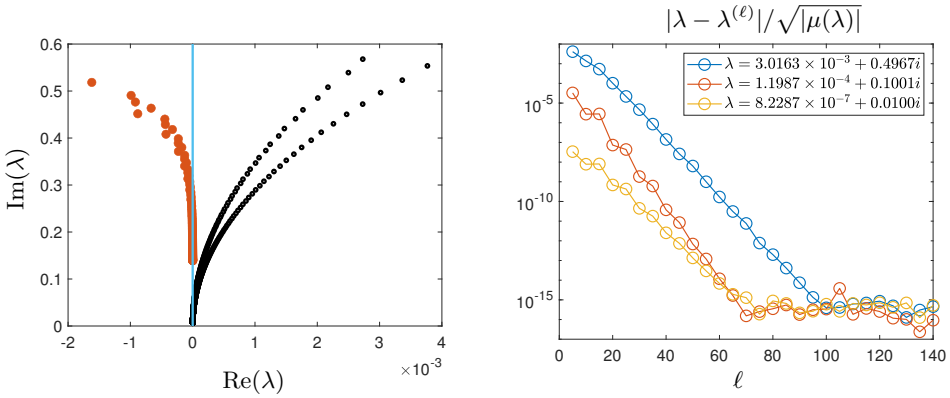

FIGURE 4.12. *Left: Eigenvalues accumulating at the essential spectral point $\lambda = 0$. Right: Relative accuracy of the InfBeyn computed eigenvalues $\lambda^{(\ell)}$ for ℓ quadrature points in (2.7). We have normalized by $\sqrt{|\mu(\lambda)|}$ to capture the different rational scalings of λ in the NEP.*

call it *ghost essential spectra*. In contrast, $\lambda = 0$ is the only point in the essential spectrum of the NEP. In the right panel of Figure 4.10, we see the accumulation of the discrete spectrum at $\lambda = 0$, which also causes issues for the discretized problem. Figure 4.11 shows a similar plot in the $\mu(\lambda)$ plane.

As a final experiment, we show a region near the essential spectrum at $\lambda = 0$ (see Figure 4.12 (left)). We see clustering of the spectrum at this point, computed using InfBeyn. On the right, we have shown convergence to three eigenvalues as the number of quadrature nodes increases, where a circular contour around several eigenvalues is used. This demonstrates the effectiveness of infinite-dimensional contour methods such as InfBeyn for problems with accumulating spectra, owing to their locality, parallelizability, and rapid convergence.

5. Conclusion. As we show with six examples, discretizing infinite-dimensional NEPs can modify, destabilize, or destroy eigenvalues. By delaying discretization, we proposed practical algorithms for computing spectra and pseudospectra of infinite-dimensional NEPs that avoid these issues, and we proved their stability and convergence. We hope that the paper generates interest in infinite-dimensional NEP solvers. For example, while InfBeyn deals with regions where the spectrum is discrete and our

method for computing pseudospectra can deal with the essential spectrum, we imagine that there is an infinite-dimensional algorithm for directly computing essential spectra of NEPs.

Contour methods are not the only method that can be extended effectively to infinite dimensions. Other methods include the infinite Arnoldi method for NEPs [56], rational approximation [48], and deflation techniques [36]. It is not clear whether one approach is inherently superior to another; this likely depends heavily on the specific problem. Some methods are also easier to formulate than others. Contour methods do offer at least one distinct advantage, though. They are often easier to analyze in infinite dimensions simply because they involve solutions of fixed infinite-dimensional linear systems (at least when one does not involve iterations of applying the contour integral operator), which facilitates proofs of properties such as convergence and stability, as demonstrated by the theorems presented in our paper. At the time of writing, it is an interesting question how other techniques must be adapted to circumvent the discretization issues discussed in this paper. We hope that this paper inspires interest in these problems.

We are also intrigued by some down-the-line applications such as reduced order models [17, 42, 70] and developing structure-preserving infinite-dimensional solvers. Infinite-dimensional NEP solvers offer the potential for more robust calculations of physically relevant spectra in challenging applications.

Acknowledgements. This work started while MJC visited Cornell University from October to December 2022. We want to thank the Cecil King Foundation and the London Mathematical Society for a Cecil King Travel Scholarship to make the extended visit possible. We also thank Karl Meerbergen for discussing the rational Krylov and contour-based methods for solving nonlinear eigenvalue problems. Agnieszka Miedlar discussed the probabilistic analysis of FEAST with us. The work of the A.T. is partially supported by the National Science Foundation grants DMS-1952757 and DMS-2045646, as well as a Simons Fellowship in Mathematics.

REFERENCES

[1] P. B. Bailey, W. N. Everitt, J. Weidmann, and A. Zettl, *Regular approximations of singular Sturm–Liouville problems*, Results in Mathematics, 23 (1993), pp. 3–22.
[2] J. P. Baker, M. Embree, and J. N. Green, *Networks of vibrating strings: A model nonlinear eigenvalue problem*, in preparation, (2023).
[3] G. Beer, *Topologies on closed and closed convex sets*, vol. 268, Springer Science & Business Media, 1993.
[4] T. Betcke, N. J. Higham, V. Mehrmann, C. Schröder, and F. Tisseur, *NLEVP: A collection of nonlinear eigenvalue problems*, ACM Trans. Math. Soft., 39 (2013), pp. 1–28.
[5] T. Betcke and L. N. Trefethen, *Reviving the method of particular solutions*, SIAM Rev., 47 (2005), pp. 469–491.
[6] W.-J. Beyn, *An integral method for solving nonlinear eigenvalue problems*, Lin. Alg. Appl., 436 (2012), pp. 3839–3863.
[7] W.-J. Beyn, Y. Latushkin, and J. Rottmann-Matthes, *Finding eigenvalues of holomorphic Fredholm operator pencils using boundary value problems and contour integrals*, Integral equations and operator theory, 78 (2014), pp. 155–211.
[8] D. Bindel and A. Hood, *Localization theorems for nonlinear eigenvalue problems*, SIAM Rev., 57 (2015), pp. 585–607.
[9] D. Bindel and M. Zworski, *Theory and computation of resonances in 1d scattering*, (2006).
[10] S. Bögli, *Convergence of sequences of linear operators and their spectra*, Integral Equations and Operator Theory, 88 (2017), pp. 559–599.
[11] S. Bögli, M. Marletta, and C. Tretter, *The essential numerical range for unbounded linear operators*, J. Func. Anal., 279 (2020), p. 108509.
[12] M. Botchev, G. Sleijpen, and A. Sopaheluwakan, *An SVD-approach to Jacobi–Davidson solution of nonlinear Helmholtz eigenvalue problems*, Lin. Alg. Appl., 431 (2009), pp. 427–

440.
[13] N. Boulle and A. Townsend, *A generalization of the randomized singular value decomposition*, in International Conference on Learning Representations, 2022.
[14] N. Boullé and A. Townsend, *Learning elliptic partial differential equations with randomized linear algebra*, Foundations of Computational Mathematics, (2022), pp. 1–31.
[15] L. Boulton, N. Boussaid, and M. Lewin, *Generalized Weyl theorems and spectral pollution in the Galerkin method*, Journal of Spectral Theory, 2 (2012), pp. 329–354.
[16] J. P. Boyd, *Traps and snares in eigenvalue calculations with application to pseudospectral computations of ocean tides in a basin bounded by meridians*, Journal of Computational Physics, 126 (1996), pp. 11–20.
[17] M. C. Brennan, M. Embree, and S. Gugercin, *Contour integral methods for nonlinear eigenvalue problems: A systems theoretic approach*, arXiv preprint arXiv:2012.14979, (2020).
[18] F. Chaitin-Chatelin and M. B. van Gijzen, *Analysis of parameterized quadratic eigenvalue problems in computational acoustics with homotopic deviation theory*, Numer. Lin. Alg. Appl., 13 (2006), pp. 487–512.
[19] Y. M. Chen, X. S. Chen, and W. Li, *On perturbation bounds for orthogonal projections*, Numer. Algor., 73 (2016), pp. 433–444.
[20] M. Colbrook, *The foundations of infinite-dimensional spectral computations*, PhD thesis, University of Cambridge, 2020.
[21] M. J. Colbrook, *Computing spectral measures and spectral types*, Communications in Mathematical Physics, 384 (2021), pp. 433–501.
[22] ———, *Computing semigroups with error control*, SIAM Journal on Numerical Analysis, 60 (2022), pp. 396–422.
[23] ———, *On the computation of geometric features of spectra of linear operators on Hilbert spaces*, Foundations of Computational Mathematics, (2022).
[24] M. J. Colbrook, *infNEP*. https://github.com/MColbrook/infNEP, 2023.
[25] M. J. Colbrook, L. J. Ayton, and M. Szőke, *Residual dynamic mode decomposition: robust and verified koopmanism*, Journal of Fluid Mechanics, 955 (2023), p. A21.
[26] M. J. Colbrook and A. C. Hansen, *On the infinite-dimensional QR algorithm*, Numerische Mathematik, 143 (2019), pp. 17–83.
[27] ———, *The foundations of spectral computations via the solvability complexity index hierarchy*, Journal of the European Mathematical Society, (2022).
[28] M. J. Colbrook and A. C. Hansen, *The foundations of spectral computations via the solvability complexity index hierarchy*, J. Euro. Math. Soc., (2022).
[29] M. J. Colbrook, A. Horning, and A. Townsend, *Computing spectral measures of self-adjoint operators*, SIAM Review, 63 (2021), pp. 489–524.
[30] M. J. Colbrook, B. Roman, and A. C. Hansen, *How to compute spectra with error control*, Phys. Rev. Lett., 122 (2019), p. 250201.
[31] M. J. Colbrook and A. Townsend, *Rigorous data-driven computation of spectral properties of Koopman operators for dynamical systems*, Communications on Pure and Applied Mathematics, (to appear).
[32] A. R. Collar and A. Simpson, *Matrices and engineering dynamics*, Ellis Horwood, 1987.
[33] E. Di Napoli, E. Polizzi, and Y. Saad, *Efficient estimation of eigenvalue counts in an interval*, Numerical Linear Algebra with Applications, 23 (2016), pp. 674–692.
[34] R. Di Prima and G. Habetler, *A completeness theorem for non-selfadjoint eigenvalue problems in hydrodynamic stability*, Archive for Rational Mechanics and Analysis, 34 (1969), pp. 218–227.
[35] T. A. Driscoll and N. Hale, *Rectangular spectral collocation*, IMA J. Numer. Anal., 36 (2016), pp. 108–132.
[36] C. Effenberger, *Robust successive computation of eigenpairs for nonlinear eigenvalue problems*, SIAM Journal on Matrix Analysis and Applications, 34 (2013), pp. 1231–1256.
[37] C. Engström and M. Wang, *Complex dispersion relation calculations with the symmetric interior penalty method*, Inter. J. Numer. Meth. Eng., 84 (2010), pp. 849–863.
[38] M. A. Gilles and A. Townsend, *Continuous analogues of Krylov subspace methods for differential operators*, SIAM Journal on Numerical Analysis, 57 (2019), pp. 899–924.
[39] I. Gohberg, S. Goldberg, and M. A. Kaashoek, *Classes of linear operators*, Birkhäuser, 1990.
[40] I. u. Gohberg and E. Sigal, *An operator generalization of the logarithmic residue theorem and the theorem of Rouché*, Mathematics of the USSR-Sbornik, 13 (1971), p. 603.
[41] J. Gopalakrishnan, B. Q. Parker, and P. Vandenberge, *Computing leaky modes of optical fibers using a FEAST algorithm for polynomial eigenproblems*, Wave Motion, 108 (2022), p. 102826.
[42] N. Gräbner, V. Mehrmann, S. Quraishi, C. Schröder, and U. von Wagner, *Numerical methods for parametric model reduction in the simulation of disk brake squeal*, ZAMM-J. Appl. Math. Mech., 96 (2016), pp. 1388–1405.
[43] K. Green and T. Wagenknecht, *Pseudospectra and delay differential equations*, J. Comput. Appl. Math., 196 (2006), pp. 567–578.
[44] R. D. Grigorieff and H. Jeggle, *Approximation von Eigenwertproblemen bei nichtlinearer*

Parameterabhängigkeit, Manuscripta Mathematica, 10 (1973), pp. 245–271.
[45] C. E. Grosch and H. Salwen, *The continuous spectrum of the Orr–Sommerfeld equation. Part 1. The spectrum and the eigenfunctions*, J. Fluid Mech., 87 (1978), pp. 33–54.
[46] L. Grubišić and A. Grbić, *Discrete perturbation estimates for eigenpairs of fredholm operator-valued functions*, Applied Mathematics and Computation, 267 (2015), pp. 632–647.
[47] S. Güttel and F. Tisseur, *The nonlinear eigenvalue problem*, Acta Numer., 26 (2017), pp. 1–94.
[48] S. Guttel, R. Van Beeumen, K. Meerbergen, and W. Michiels, *NLEIGS: A class of fully rational Krylov methods for nonlinear eigenvalue problems*, SIAM Journal on Scientific Computing, 36 (2014), pp. A2842–A2864.
[49] N. Halko, P.-G. Martinsson, and J. A. Tropp, *Finding structure with randomness: Probabilistic algorithms for constructing approximate matrix decompositions*, SIAM review, 53 (2011), pp. 217–288.
[50] I. Harari, K. Grosh, T. Hughes, M. Malhotra, P. Pinsky, J. Stewart, and L. Thompson, *Recent developments in finite element methods for structural acoustics*, Arch. Comput. Meth. Eng., 3 (1996), pp. 131–309.
[51] D. J. Higham and N. J. Higham, *Structured backward error and condition of generalized eigenvalue problems*, SIAM J. Matrix Anal. Appl., 20 (1998), pp. 493–512.
[52] N. J. Higham, D. S. Mackey, F. Tisseur, and S. D. Garvey, *Scaling, sensitivity and stability in the numerical solution of quadratic eigenvalue problems*, Inter. J. Numer. Meth. Eng., 73 (2008), pp. 344–360.
[53] N. J. Higham and F. Tisseur, *More on pseudospectra for polynomial eigenvalue problems and applications in control theory*, Lin. Alg. Appl., 351 (2002), pp. 435–453.
[54] A. Horning and A. Townsend, *Feast for differential eigenvalue problems*, SIAM J. Numer. Anal., 58 (2020), pp. 1239–1262.
[55] E. Jarlebring, *The spectrum of delay-differential equations: Numerical methods, stability and perturbation*, PhD thesis, 2008.
[56] E. Jarlebring and S. Güttel, *A spatially adaptive iterative method for a class of nonlinear operator eigenproblems*, Electronic Transactions on Numerical Analysis, 41 (2014), pp. 21–41.
[57] H. Jeggle and W. Wendland, *On the discrete approximation of eigenvalue problems with holomorphic parameter dependence*, Proc. Roy. Soc. Edin. Sec. A: Math., 78 (1977), pp. 1–29.
[58] T. Kato, *Perturbation theory for nullity, deficiency and other quantities of linear operators*, J. d'Analyse Math., 6 (1958), pp. 261–322.
[59] T. Kato, *Perturbation Theory for Linear Operators*, vol. 132, Springer Science & Business Media, second ed., 1976.
[60] M. V. Keldysh, *On the characteristic values and characteristic functions of certain classes of non-self-adjoint equations*, in Dokl. Akad. Nauk SSSR, vol. 77, 1951, pp. 11–14.
[61] ———, *On the completeness of the eigenfunctions of some classes of non-selfadjoint linear operators*, Uspekhi matematicheskikh nauk, 26 (1971), pp. 15–41.
[62] J. Kestyn, E. Polizzi, and P. T. Peter Tang, *FEAST eigensolver for non-Hermitian problems*, SIAM J. Sci. Comput., 38 (2016), pp. S772–S799.
[63] V. Kozlov and V. Maz'ya, *Differential equations with operator coefficients: with applications to boundary value problems for partial differential equations*, Springer Science & Business Media, 1999.
[64] Z. Kukelova, M. Bujnak, and T. Pajdla, *Polynomial eigenvalue solutions to the 5-pt and 6-pt relative pose problems.*, in BMVC, vol. 2, 2008, p. 2008.
[65] P. Lancaster, *Lambda-matrices and vibrating systems*, Courier Corporation, 2002.
[66] B.-S. Liao, Z. Bai, L.-Q. Lee, and K. Ko, *Nonlinear Rayleigh–Ritz iterative method for solving large scale nonlinear eigenvalue problems*, Taiwanese J. Math., 14 (2010), pp. 869–883.
[67] D. Marcuse, *Theory of dielectric optical waveguides*, Elsevier, 2013.
[68] A. Markus and E. Sigal, *The multiplicity of the characteristic number of an analytic operator function*, Mat. Issled, 5 (1970), p. 17.
[69] V. Mehrmann and C. Schröder, *Nonlinear eigenvalue and frequency response problems in industrial practice*, J. Math. Ind., 1 (2011), pp. 1–18.
[70] ———, *Eigenvalue analysis and model reduction in the treatment of disc brake squeal*, SIAM News, 49 (2016), pp. 1–3.
[71] V. Mehrmann and D. Watkins, *Polynomial eigenvalue problems with Hamiltonian structure.*, Electr. Trans. Numer. Anal., 13 (2002), pp. 106–118.
[72] R. Mennicken and M. Möller, *Root functions, eigenvectors, associated vectors and the inverse of a holomorphic operator function*, Archiv der Mathematik, 42 (1984), pp. 455–463.
[73] ———, *Non-self-adjoint boundary eigenvalue problems*, vol. 192, Gulf Professional Publishing, 2003.
[74] W. Michiels, K. Green, T. Wagenknecht, and S.-I. Niculescu, *Pseudospectra and stability radii for analytic matrix functions with application to time-delay systems*, Lin. Alg.

Appl., 418 (2006), pp. 315–335.
[75] S. Olver, *GMRES for the differentiation operator*, SIAM journal on numerical analysis, 47 (2009), pp. 3359–3373.
[76] S. Olver and A. Townsend, *A fast and well-conditioned spectral method*, SIAM Rev., 55 (2013), pp. 462–489.
[77] S. A. Orszag, *Accurate solution of the Orr–Sommerfeld stability equation*, J. Fluid Mech., 50 (1971), pp. 689–703.
[78] S. C. Reddy, P. J. Schmid, and D. S. Henningson, *Pseudospectra of the Orr–Sommerfeld operator*, SIAM J. Appl. Math., 53 (1993), pp. 15–47.
[79] M. Reed and B. Simon, *Methods of Modern Mathematical Physics I: Functional Analysis*, Academic Press, second ed., 1980.
[80] K. Sakoda, N. Kawai, T. Ito, A. Chutinan, S. Noda, T. Mitsuyu, and K. Hirao, *Photonic bands of metallic systems. I. Principle of calculation and accuracy*, Phys. Rev. B, 64 (2001), p. 045116.
[81] F. W. Schäfke and A. Schneider, *S-hermitesche rand-eigenwertprobleme. I*, Mathematische Annalen, 162 (1965), pp. 9–26.
[82] P. J. Schmid, D. S. Henningson, and D. Jankowski, *Stability and transition in shear flows. applied mathematical sciences, vol. 142*, Appl. Mech. Rev., 55 (2002), pp. B57–B59.
[83] S. I. Solov'ev, *The finite-element method for symmetric nonlinear eigenvalue problems*, Zhurnal Vychislitel'noi Matematiki i Matematicheskoi Fiziki, 37 (1997), pp. 1311–1318.
[84] S. I. Solov'ëv, *Preconditioned iterative methods for a class of nonlinear eigenvalue problems*, Lin. Alg. Appl., 415 (2006), pp. 210–229.
[85] O. Steinbach and G. Unger, *A boundary element method for the Dirichlet eigenvalue problem of the Laplace operator*, Numer. Math., 113 (2009), pp. 281–298.
[86] D. Stowell and J. Tausch, *Variational formulation for guided and leaky modes in multilayer dielectric waveguides*, Comm. Comput. Phys., 7 (2010), p. 564.
[87] F. Tisseur, *Backward error and condition of polynomial eigenvalue problems*, Lin. Alg. Appl., 309 (2000), pp. 339–361.
[88] F. Tisseur and N. J. Higham, *Structured pseudospectra for polynomial eigenvalue problems, with applications*, SIAM J. Matrix Anal. Appl., 23 (2001), pp. 187–208.
[89] A. Townsend and L. N. Trefethen, *Continuous analogues of matrix factorizations*, Proc. Roy. Soc. A: Math., Phys. Eng. Sci., 471 (2015), p. 20140585.
[90] L. N. Trefethen, *Computation of pseudospectra*, Acta Numer., 8 (1999), pp. 247–295.
[91] L. N. Trefethen and M. Embree, *Spectra and pseudospectra: the behavior of nonnormal matrices and operators*, Princeton University Press, 2005.
[92] V. Trofimov, *The root subspaces of operators that depend analytically on a parameter*, Mat. Issled, 3 (1968), pp. 117–125.
[93] G. Vainikko, *Funktionalanalysis der diskretisierungsmethoden*, Teubner-Texte zur Mathematik, (1976).
[94] G. Vainikko, *Approximative methods for nonlinear equations (two approaches to the convergence problem)*, Nonlinear Analysis: Theory, Methods & Applications, 2 (1978), pp. 647–687.
[95] G. Vainikko, *Gmres and discrete approximation of operators*, Proc. Estonian Acad. Sci. Phys. Math., 53 (2004), pp. 124–131.
[96] H. Voss, *A rational spectral problem in fluid-solid vibration*, Preprints des Institutes für Mathematik, (2002).
[97] T. Wagenknecht, W. Michiels, and K. Green, *Structured pseudospectra for nonlinear eigenvalue problems*, J. Comput. Appl. Math., 212 (2008), pp. 245–259.
[98] M. Webb, *Isospectral Algorithms, Toeplitz Matrices and Orthogonal Polynomials*, PhD thesis, University of Cambridge, 2017.
[99] M. Webb and S. Olver, *Spectra of Jacobi operators via connection coefficient matrices*, Communications in Mathematical Physics, 382 (2021), pp. 657–707.
[100] J. Weidmann, *Lineare Operatoren in Hilberträumen: Teil 1 Grundlagen*, Springer-Verlag, 2013.